On the hygrothermal behavior of concrete containing glass powder and silica fume

Fouad Boukhelf, Rachid Cherif, Abdelkrim Trabelsi, Rafik Belarbi, Mohamed Bachir Bouiadjra

On the hygrothermal behavior of concrete containing glass powder and silica fume

Fouad BOUKHELF[a,b,c], Rachid CHERIF[a], Abdelkrim TRABELSI[d], Rafik BELARBI[a,b*], Mohamed BACHIR BOUIADJRA[c]

[a] LaSIE, UMR CNRS 7356, La Rochelle University, Av Michel Crépeau, 17042 La Rochelle Cedex 1, France
[b] 4evLab, LaSIE, CNRS, EDF R&D, La Rochelle University, Avenue Michel Crépeau 17042, La Rochelle Cedex1, France
[c] Laboratoire des Structures et Matériaux Avancés dans le Génie Civil et Travaux Publics, University of Sidi Bel Abbes, Faculty of Technology, Civil Engineering Department, Algeria.
[d] Univ Lyon, CNRS, INSA-Lyon, Université Claude Bernard Lyon 1, CETHIL UMR5008, F-69621 Villeurbanne, France.
[*] Corresponding author: LaSIE, UMR CNRS 7356, University of La Rochelle, Av Michel Crépeau, 17042 La Rochelle Cedex 1, France. Tel: +33 (0)5 46 45 72 39. Email: rbelarbi@univ-lr.fr

Abstract

In this work, the effect of the partial replacement of cement by alternatives derived from waste glass and silica fume on the hygrothermal behavior of concrete was investigated. For this purpose, concretes containing 20% and 30% of glass powder (GP) have been tested. In addition, two concretes containing the same replacement ratios of GP and 5% of silica fume (SF) were also manufactured. The mixtures were characterized in terms of workability, compressive strength, microstructure and hygrothermal properties. The results show that the use of 20% and 30% of GP improves the consistency of the concrete in the fresh state by 41% and 55%, respectively. In the hardened state, the use of GP engenders an increase in porosity and slightly affects the pore size distribution. However, the SF reduces the critical diameter and creates a range of micropores. Despite the decrease of compressive strength with increasing GP ratio, the concrete exhibits satisfactory performance for structural application at both 28 days (36–41 MPa) and 91 days (40–45 MPa). The cement substitution by 30% of GP and 5% of SF highlights a decrease in thermal conductivity and the specific heat of about 17% and 2.3%, respectively. The water vapor permeabilities of the concrete used ranged from 2.07e-12 to 4.74e-12 kg/m.s.Pa.

Keywords

Glass waste; Silica fume; Microstructure; Hygrothermal properties; Concrete.

1. Introduction

With about 100 billion cubic meters per year, concrete is the most widely used building material in the world (Gencel et al., 2021; Miller et al., 2016). It is responsible for 5.2% of global greenhouse gas emissions mainly due to the manufacturing process of cement, which requires a very high firing temperature to form the clinker (WBCSDIEA, 2009). This is in contradiction with the sustainable development requirements, which are becoming more and more stringent. Therefore, on the path to ensuring environmental sustainability, it is crucial to consider ways to further reduce the carbon impact of this material.

Among the proposed solutions, the use of mineral additions, such as silica fume, blast furnace slag and fly ash, to replace the cement in concrete is a promising method to minimize the environmental impact of the cement industry (Berenguer et al., 2020; Feldman, 1981; Manmohan, D. and Metha, 1981; Sellevold et al., 1982; Shen et al., 2020; Zemri and Bachir Bouiadjra, 2020). Beyond environmental aspects, in several works (Antoni et al., 2015; Bani Ardalan et al., 2017), it has been argued that the use of mineral additions improves the consistency of concrete and its mechanical properties and enhances its durability. Moreover, from a hygrothermal point of view, recent studies underlined that incorporating fly ash (Bentz and Peltz, 2011; Demirboğa, 2007) and silica fume (Gökçe et al., 2019) as partial cement replacement in concrete resulted in the reduce of its thermal conductivities and increase of its specific heats and mass transfer parameters such as sorption isotherms and water vapor permeability (Issaadi et al., 2015). While recognizing that the use of silica fume constitutes a widespread application, research on other additions resulting from waste recovery as a substitute for cement remains a challenge for construction engineers. More recently, the incorporation of glass waste in concrete has been widely used because of the economic and environmental issues (Bouchikhi et al., 2019; Chandra Paul et al., 2018; Du et al., 2021; Mohajerani et al., 2017; Oliveira et al., 2015; Xiao et al., 2021; Yang et al., 2019). The motivations are the physical and chemical properties of glass powder, which are relatively similar to those of the additional cement materials (Tan and Du, 2013). Although glass powder can be used as an additional cement material, a lack of data in the literature is one of the principal obstacles preventing it from reaching the same commercial success as other mineral additions.

Over the past two decades and in order to preserve natural resources, the use of glass waste as fine or coarse aggregate in concrete has been widely studied in the literature (Aliabdo et al., 2016; Chandra Paul et al., 2018; Federico and Chidiac, 2009; Gerges et al., 2018; Mohajerani et al., 2017; Penacho et al., 2014; Rashad, 2015, 2014). When the glass is used as an aggregate, its high alkali content generates an alkali–silica reaction (ASR) that causes damaging stresses and cracks in the concrete (Shayan and Xu, 2004). Based on research conducted by (Gerges et al., 2018), it was concluded that the incorporation of fine aggregates at percentages below 30% improves the long-term compressive strength. On the other hand, the addition of these aggregates exhibits a rather negative effect beyond 30%, where it reduces the mechanical properties of the concrete. In fact, the lessening of the mechanical properties for a high amount of glass could be attributed to the angular nature of glass particles (Bisht and Ramana, 2018), which affects the quality of the Interfacial Transition Zone “ITZ” between the aggregate and cementitious matrix.

In addition, several researchers highlighted that reducing the glass size as much as possible reduces the ASR reaction and concrete damage and increases the pozzolanic reactions, which enhances the mechanical properties of the concrete (Serpa et al., 2013; Shayan and Xu, 2004; Zidol et al., 2017). The use of less than 30% of glass powder as cement replacement in concrete, in particular, glass powder particles below 75 microns, reduces the ASR and concrete expansion (Idir et al., 2011, 2010;

Shao et al., 2000; Shayan and Xu, 2004; Taha and Nounu, 2008; Zidol, 2009). Furthermore, it has been shown that the finer the glass powder obtained from grinding glass bottles further develops the pozzolanic properties, reduce the alkali–silica reaction (ASR) (Khmiri et al., 2013; Samtur, 1974; Shayan and Xu, 2006; Vaitkevičius et al., 2014), enhances mechanical performance and can be used as a cement substitute for construction (Idir et al., 2011; Shayan and Xu, 2006, 2004; Zidol, 2009).

In addition to the advantages offered by the use of fine glass waste with regard to the properties in the hardened state, the partial replacement of cement by glass powder improves the properties in the fresh state, so it can be used to make high-strength concrete without using other superplasticizers (Meyer et al., 2001). From a sustainability point of view, De Castro and De Brito (2013) have found that the use of glass powder as a replacement for cement does not significantly alter the durability-related properties of concrete. Besides the mechanical and fresh properties, which have been sufficiently discussed in the literature, recent works (Chand et al., 2021; Du et al., 2021; Yang et al., 2019) has attempted to evaluate the thermal conductivity and durability of concrete containing glass powder.

In spite of the growing attention paid to the valorization of waste glass in concrete, the hygrothermal properties of these materials are rarely studied in the existing literature. Recently, Yang et al., (2019) studied the effect of waste glass as a total sand replacement on the thermal conductivity and compressive strength of concrete exposed to fire. The thermal conductivity and density of the mortars decreased slightly as the particle size of the glass aggregates decreased. Furthermore, the use of glass improves the compressive strength after fire exposure. Du et al., (2021) evaluated the thermal conductivity of cement paste containing up to 25% of glass waste fine aggregate. The results highlighted that the greater the amount of glass, the lower the thermal conductivity of the mixtures. At 25% of glass, a diminution of 24% of the thermal conductivity was noticed compared to the reference paste without glass replacement. Experimental investigations showed a good behavior of concrete with glass powder towards the thermal conductivity (Guo et al., 2020) and water permeability (Hussain, 1994; Rahman, 2015; Zidol, A., Pavoine, A. and Tagnit-Hamou, 2012; Zidol et al., 2017).

A promising way to address the requirements of the RE2020 environmental regulation in terms of greenhouse gas emission reduction and sustainable construction in the building sector is the use of solid waste glass and silica fume as partial replacement of cement. Use of silica fume can be expected to avoid problems associated to the low mechanical strength at short term. To be precise, the glass powder and silica fume incorporated in concrete is both beneficial to environmental protection and economic development while keeping/improving the mechanical and hygrothermal performance of the material. To the best of our knowledge, researches dealing with the partial replacement of cement by glass powder and silica fume have been limited to the mechanical and durability properties.

The objective of this work is to investigate the impact of the microstructural properties of concretes with glass powder and silica fume on their intrinsic properties; it concerns the mechanical properties in addition to the thermal and hydric properties. The hydric aspect directly intervenes on the durability of materials, since water, in its various forms, is the main vector of transport of aggressive species such

as sulfates and chlorides. It is also the seat of chemical reaction of carbonation phenomenon. Moreover, in the perspective of an application of its materials in construction and renovation, it is important to know the thermal properties, to reach the regulation requirements. An experimental investigation has been carried out which considers all these aspects.

For this purpose, heat and mass transfer parameters such as water vapor permeability, sorption isotherms, thermal conductivity and specific heat were evaluated. In addition, aiming to understand the phenomena that govern hygrothermal transfer, this experimental investigation was complemented by a microstructure characterization of the material by means of water and mercury porosimetry, scanning electron microscopy in environmental mode (E-SEM) and thermogravimetric analysis. The results obtained will be useful when predicting the hygrothermal behavior of building envelopes based on these concretes. This study is part of the environmental transition and sustainable construction. They will also allow the identification of possible risks of disorders related to excessive humidity and help predict the durability of building materials and structures (steel corrosion).

2. Experimental program

The experimental investigation was undertaken with the aim of concretizing the link between the consistency, mechanical and hygrothermal properties and the substitution of a fraction of cement, which is responsible for significant greenhouse gas emissions, by other non-biodegradable greenhouse alternatives, that is, glass powder, which constitutes large amounts of waste.

In a first step, a characterization of the binder constituents was performed through particle size analysis, scanning electron microscopy (SEM) and reactivity analysis of the powders used. After that, concretes with Portland cement (CEMI), glass powder (GP) and silica fume (SF) were mixed. Several replacement ratios of cement by GP and SF were addressed. A microstructural characterization of the tested concretes was undertaken using water and mercury porosimetry, SEM and thermogravimetry analyses (TGA). In addition to that, the workability and mechanical strength of these concretes were assessed and compared to a control concrete with CEMI (Ref).

Finally, the hygrothermal characterization of the concretes used were performed and analyzed in relation to their microstructural properties. The experimental investigations cover the study of the thermal conductivity, specific heat, vapor permeability and sorption isotherms.

2.1. Materials

The cement type used is CEMI 52.5N in compliance with the European standard EN 197-1 (2012). Silica fume in compliance with the European standard EN 13263-1 (2005) and glass powder were used as mass substituents of the CEMI. The glass powder was recovered from glass waste of different colours, provided by the waste disposal plant of La Rochelle agglomeration (France). The procedure used for preparing the glass powder was first to clean the collected waste glass from any impurities by immersion in water for 7 days. During this period, the water was changed every day. After cleaning, the crushing was repeated until achieving a glass powder diameter < 50 µm as shown in Fig. 1.

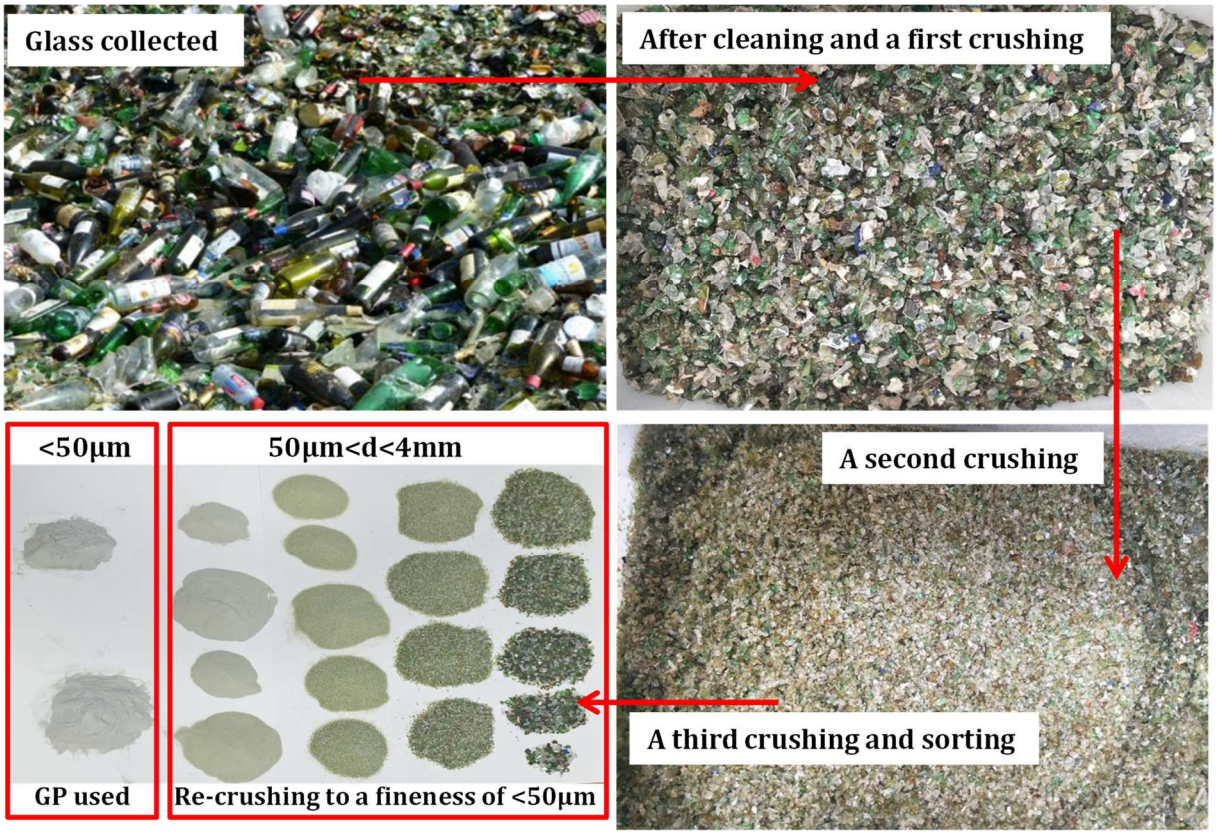

Fig 1: Preparation of waste glass powder.

For this study, five concrete mixtures were proposed as shown in Table 1. All mixtures have a water to binder ratio (W/B) of 0.45, with 350 kg/m^3 of binder. Firstly, a control concrete based only on CEMI was manufactured (called Ref).

Then, four concretes containing glass powder (GP) as a partial mass replacement of CEMI were used: (i) 20% of glass powder (called 20G-I); (ii) 30% of glass powder (30G-I), these two ratios being based on the literature (Zidol et al., 2017). Secondly, two other concretes with partial mass replacement of cement with glass powder and mineral addition of silica fume SF were produced: (iii) 20% of glass powder and 5% of silica fumes (20GSF-I) and (iv) 30% of glass powder and 5% of silica fumes (30GSF-I), where SF was added in order to refine the microstructure which could prove the durability and hygrothermal performances of the concretes. In fact, (Perraton et al., 1988) suggest that it is preferable to substitute between 5 and 10% of the cement mass with silica fume; beyond 8%, the substitution is useless and the material performance decreases. A SikaCem® superplasticizer was added to all the mixtures of 2 l/m^3 in order to obtain a better consistency. Finally, sand (0/4 mm) and gravel (4/12.5 mm) were used for all the concrete studied. We noted that the mix design of concretes and mass substitutions used were based on the previous studies in the literature in order to compare it with our results (Bouchikhi et al., 2019; Islam et al., 2017; Matos and Sousa-Coutinho, 2012; Zidol et al., 2017). The formulations of concretes with GP and SF are calculated from the approach previously used by (Khokhar et al., 2010) considering the densities of all the raw materials and keeping the same W/B ratio and paste volume for all the concretes used.

Table 1: Mix design of concretes studied (kg/m^3).

Formulations	Density (kg/m^3)	Ref	20G-I	30G-I	20GSF-I	30GSF-I
Sand 0/3.15	2490	639	639	639	639	639
Gravel 3.15/12.5	2310	1070	1070	1070	1070	1070
Cement	3170	350	282.9	258.2	271.2	248.4
Glass powder	2180	0	56.6	77.5	54.2	74.5
Silica fume	2710	0	0	0	13.6	12.4
Water	1000	157.5	152.8	151.0	152.6	150.9
W/B	-	0.45	0.45	0.45	0.45	0.45
Clinker ratio (%)	-	95	77	70	74	67

2.2. Tests and protocols

2.2.1 Raw material analysis

Particle size analysis of each binder used was carried out using a dry method with the CILAS 1090 particle-size-analyser® device in compliance with NF EN 933-1 (2012), which can detect particle sizes from 0.1 µm to 2 mm. The specific surface measured by BET method based in Brunauer, Emmett et Teller theory and in compliance with standard EN ISO 18757 (2006) of raw materials were performed. The heat flow was measured using a TAM air-insulated calorimeter®, containing eight separate measuring cells in compliance with ASTM C1702 (2017). The glass vial was sealed and placed in the calorimeter, and the heat flow was measured for about 25 h. During the test, isothermal conditions of 20°C ± 0.02°C were maintained in the measuring cells. Isothermal calorimetry was performed to investigate the pozzolanic reaction of the GP and SF on cement hydration at an early age.

2.2.2. Workability

The Abrams cone slump test is most commonly used to determine the fresh concrete workability. This test is carried out in compliance with the recommendations in NF EN 12350-2 (2012). In this test, workability is characterized by the slump of a concrete cone under its own weight. The standard NF EN 206 (2016) defines five consistency classes according to the measured slump: firm, plastic, very plastic, fluid and very fluid.

2.2.3. Water and mercury porosimetry

Water porosity tests were carried out in compliance with the recommendations of AFPC-AFREM (2007) The porosity (Φ) can be obtained by Eq. (1):

$$\Phi = \frac{M_{air} - M_{dry}}{M_{air} - M_{water}} \times 100\% \quad (1)$$

where M_{air} and M_{water} are the weight mass of the saturated sample weighed in air and in water respectively. M_{dry} is the dry mass of the tested sample. For each concrete, the average water porosity and its standard deviation from three measurements were measured at 91 days.

In order to study the effect of the glass powder and silica fume on the pore size distribution and the

transfer parameters of the concretes tested, mercury intrusion porosimetry was performed on a sample size of 3 cm^3 at 3 months of curing. It was carried out using an Autopore V 9600 from Micromeritics® in compliance with the standard ASTM D4404–84 (1998). Its injection pressure was higher than 400 MPa.

2.2.4. Compressive strength

The compressive strength at 28 and 91 days was measured on three different cylindrical specimens measuring 11 cm in diameter and 22 cm in height in compliance with the European standard EN 12390-3 (2019). The specimens were demoulded after 24 hours of manufacturing and stored in a humid chamber at 50% RH and a temperature of 22°C. These conditions (air-curing), widely used in the literature (Younsi et al., 2011), better simulate the reality than water-curing and avoid the material leaching in water.

2.2.5. Scanning electron microscopy (SEM)

SEM imaging was carried out by using an environmental FEI Quanta 200 ESEM FEG, equipped with a FEG Field Effect GUN electron emitter, and Large Field Detector (LFD) of Secondary Electrons (SE). The device was operated at 20 kV and 1.5 mbar in water vapor pressure. The advantage of this technique is that no sample preparation is required before the test, which can affect its morphology, and to preserve it from damage (Cherif et al., 2020; Conforto et al., 2015).

2.2.6. Thermogravimetric analysis TGA

Thermogravimetry is an analytical technique that involves measuring the mass variation of a sample as a function of temperature. In our case, this technique was used to monitor the solid phase formations of the concretes and the possible pozzolanic reaction ($Ca(OH)_2$, calcite, etc.). The device used was the SETARAM® type SETSYS Evolution 16/18. It consists of a sealed chamber to control the atmosphere of the sample by injection of argon gas, an oven to manage the temperature, a weighing module (microbalance), a thermocouple to measure the temperature, and a computer to control and record data. During the test, the temperature should be increased from the ambient to a temperature of 1000°C with a constant velocity of 10°C/min. The latter are widely used in the literature and recommended by (AFPC-AFREM, 2007; Santos et al., 2020).

2.2.7. Specific heat

The specific heat was measured by using the calorimeter Calvet BT 2.15® device in compliance with the standard NF EN 821-3 (2005). The advantage of this device is that the 3D Calvet sensor completely surrounds the sample, such that all the heat emitted is measured.

The calorimeter consists of a reference cell containing a thermally inert product and a measuring cell in which the test sample is placed. Cells are fitted with a socket and a three-dimensional flow meter. They are specially used for solids or powdered materials with low vapor pressure with an internal pressure of up to 500 kPa. The amount of heat exchanged by the sample is measured by the 3D flow meter, which allows the specific heat to be deduced. The heat change follows three sequences: (i) constant temperature of -10°C for 12 hours, (ii) a ramp from -10°C to 45°C with a velocity of

0.1°C/min, and (iii) constant temperature of 45°C for 3 hours. The samples analyzed followed the same protocol of post-fabrication preservation and pre-conditioning prior to the test: preservation in a wet room for 24 hours after manufacture (RH = 50% and T = 22°C) for 28 days of curing, after which they are dried in an oven at 40°C until equilibrium.

2.2.8. Thermal conductivity

The thermal conductivity was measured, under stationary conditions, for a controlled temperature of the samples at 23°C), using the λ-Meter EP 500e® device based on the guarded hot plate method in compliance with the European standards (EN 12664, 2001; EN 12667, 2001). The test involves placing a sample of 15x15x5 cm between a cold and hot plate, i.e. the sample is subjected to a given temperature gradient. A guard ring around the measuring area ensures the unidirectional transfer through the sample thickness. Then, the thermal conductivity is calculated from the electrical power supplied using Eq. (2).

$$\lambda = \frac{Q.e}{\Delta T.A} \qquad (2)$$

where e (m) is the sample thickness; A (m^2) is the area of the sample; ΔT (K) is the temperature gradient between the two plates and Q (W) the electric power.

2.2.9. Sorption isotherm

The sorption–desorption isotherms present the capacity of the material to capture or retain water with relative humidity variation (RH) for a constant temperature in compliance with ISO 12571 (2000).

The method used to determine the sorption–desorption curves is the gravimetric method using the ProUmid® device. It is based on the regular monitoring of the gain or loss of the sample mass as a function of the RH ranges. For each range, weighing is performed until equilibrium is reached.

2.2.10. Water vapor permeability

The coefficient of water vapor permeability is determined by the Cup method in compliance with the European standard ISO 12572 (2001). The test is carried out using the Gravitest® device, which is composed of 6 cups in a controlled climatic chamber and a high balance precision (10^{-4} g) for the mass monitoring. Indeed, a gradient vapor pressure is applied, under isothermal conditions, between the interior of the cup and the climatic chamber, i.e., between the two faces of the tested sample. The flow ratio was evaluated by regularly weighing each cup including the material. In order to determine the equilibrium water vapor transmission ratio and the water vapor permeability, regular de-weighing of the cup and sample were automatically carried out.

3. Results and discussion

3.1. Raw material characterization

Table 2: Physical properties of cement, silica fume and glass powder used.

	CEMI 52.5 N	Silica fume	Glass powder
d_{10} (µm)	3.2	2	11
d_{50} (µm)	12	8.5	19
d_{90} (µm)	28	18	34
d_{max} (µm)	60	36	50
Density (kg/m^3)	3170	2180	2710
BET specific surface area (m²/g)	6.43	22.07	5.65

The results are given in Fig. 2. The diameters d_{10}, d_{50} and d_{90}, density and BET specific surface area BET of the powders used are illustrated in Table 2. The silica fume (SF) was also designed with a density of 2180 kg/m^3 and a maximum particle size (d_{max}) of 36 µm. The glass powder (GP) presents a density of 2710 kg/m^3 and d_{50} of 19 µm. The particle size distribution of the cement was continuous, being finer than GP and coarser than SF.

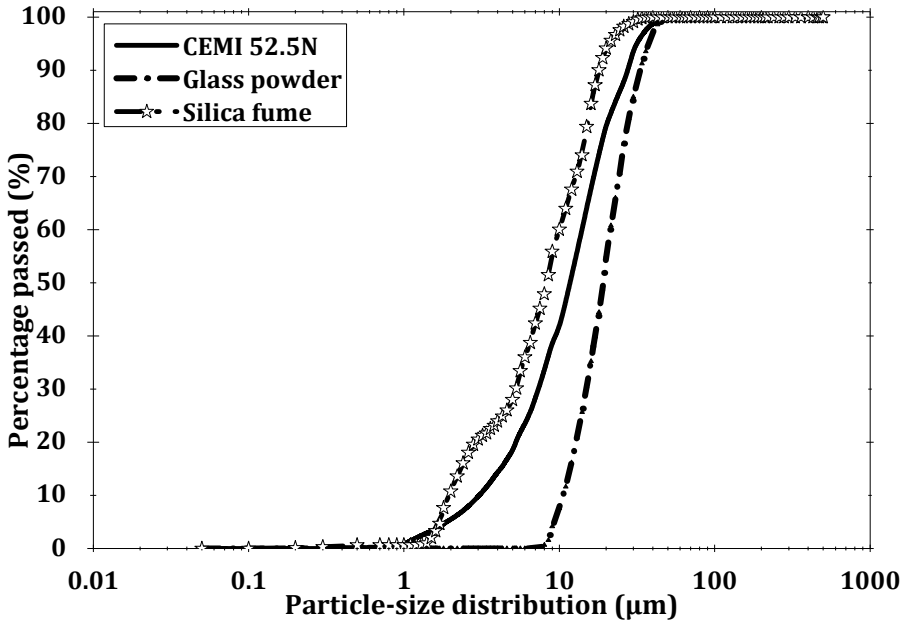

Fig. 2: Particle-size distribution of cement, glass powder and silica fume.

The SEM images in Fig. 3 show the morphology and size particles of the CEMI, GP and SF. Obviously, the CEMI and SF consist of multi-size and multi-phase powder particles, irregularly shaped for the CEMI, contrary to the SF powder. In addition, the SF contains finer particles of the order of 50 nm stacked on large particles as shown in Fig. 3-b. The particle sizes range from 1 µm to 60 µm for the CEMI and SF as shown in Fig. 2. The GP has multi-size and irregular shaped particles, ranging from 8 µm to 50 µm as shown in Table 2. The elemental analysis by weight percentage of the binders, performed by energy dispersive X-ray micro-analysis (EDX) coupled to SEM at a spot, is shown in Table 3. It allows the chemical elements of the materials used to be identified and quantified. The results show that the glass powder and silica fume are rich in silica. The latter are responsible for

283 the pozzolanic reaction of both the binders and the formation of more C-S-H, to the detriment of
284 portlandite (Urhan, 1987a, 1987b), which participates to improve the material durability.

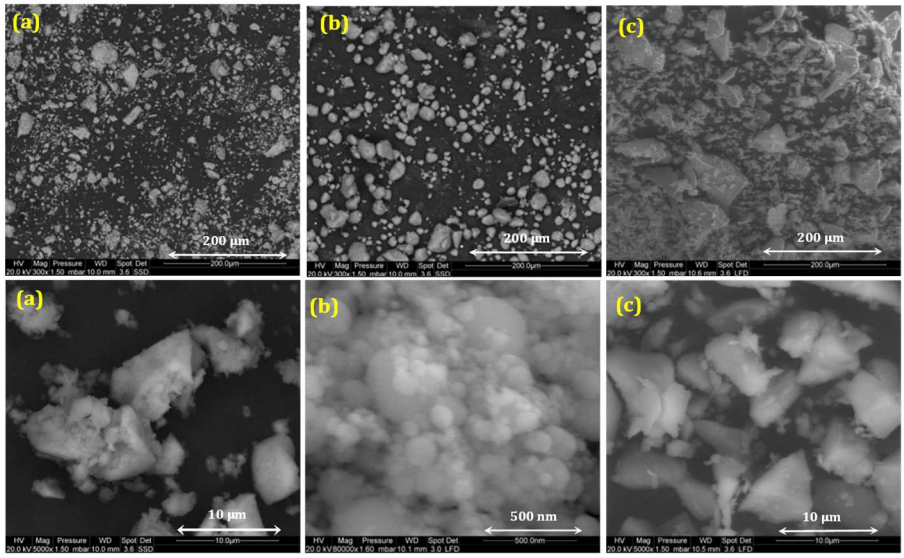

285
286 Fig. 3: SEM images of CEMI (a), silica fume (b) and glass powder (c).

287 Table 3: Elemental composition of the binders used (% wt).

	C	O	Na	Mg	Al	Si	S	K	Ca	Fe
CEMI	47.06	20.55	0	0.31	3.06	5.01	0.4	0.41	22.42	0.78
Silica fume	32.74	43.92	0	0	1	22.34	0	0	0	0
Glass powder	8.67	43.36	7.7	1.19	4.17	28.83	0	0.53	5.55	0

288 The rate of hydration represented in the heat emission curve of the materials studied with 0%,
289 20%, and 30% GP replacements within the first 25 h after contact between the water and
290 cementitious materials contact, normalized to the total binder weight in the mixture, are shown in
291 Fig. 4. It is clear that the maximum heat flow was reduced as the cement replacement with GP and
292 SF increased. Fig. 4 show that the maximum value of the second exothermic peak of 20G-I, 30G-
293 I, 20GSF-I and 30GSF-I were 14.6%, 22%, 29.2% and 31.7% lower, respectively, compared to
294 REF. The reduction in the rate of heat evolution was due to the dilution of the cement (reduction
295 in overall volume of the cementitious materials) and, consequently, the hydration products. The
296 pozzolanic reaction of GP generates less heat than cement because the reaction is similar to that of
297 C_2S. The results of this study are consistent with previous findings (Dyer and Dhir, 2001) and
298 allows to better discuss the obtained results for the mechanical and hygrothermal characterization.

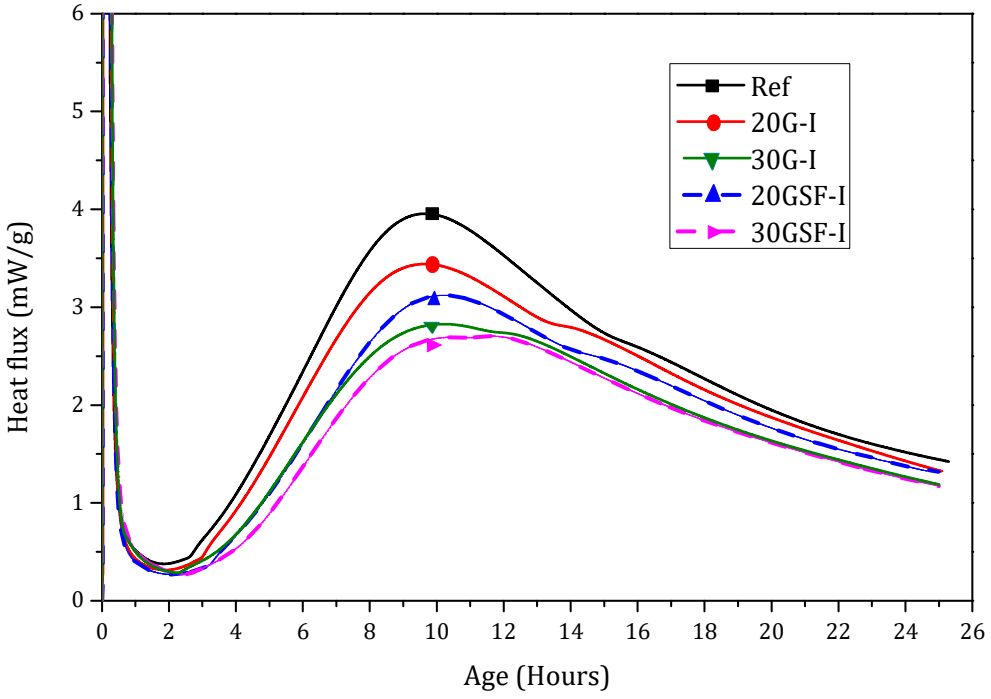

Fig. 4: Hydration process of binders used.

3.2. Workability

Fig. 5 shows the slump values for the studied concretes measured at the time of elaborating. The results obtained showed that the slump of the tested concretes varies between 129 and 200 mm. Moreover, for concretes only with GP (20 G-I) and (30 G-I), the addition of GP led to an improvement of up to 55%, thus changing the concrete's consistency from very plastic (for the control concrete Ref) to fluid for concretes with GP. The lower fineness of GP led to higher workability because of its smaller specific surface area BET and low water demand for hydration. This result seems to be in good agreement with those found previously by (Raju et al., 2020), which underlined that the use of glass powder increased the workability of concrete due to the fineness of the GP (BET area of 5.65 m^2/g) which is lower than that of CEM I used (of 6.43 m^2/g). Therefore, the substitution of cement by GP decreases the water demand for hydration i.e., increases the amount of free water and the workability of the concretes. Furthermore, the workability increases with the amount of GP used (20% GP and 30% GP). For concretes with GP (20% and 30%) and silica fume (5%), workability also decreased compared to the control concrete (Ref), despite the presence of silica fume which is supposed to absorb water and increase water demand in the mix due to its fineness (of 22.07 m^2/g and d_{max} =36µm). This is due to the presence of GP in large quantity (compared to SF) and with a much lower fineness which decreased the water demand for hydration and increased the workability compared to Ref with only CEMI. Finally, the increase in workability of G-I concretes remains lower than that of GSF-I due to the presence of silica fume. This is in agreement with the literature (Bueno et al., 2020; Chand et al., 2021). That is why we do not insist on the comparison between the slumps of

materials to discuss their properties. Further investigation on concretes with the same fineness of the blinder and the same workability could be useful to monitor their feasibility.

Furthermore, the improvements obtained make the workability of the concrete easier while reducing the costs related to the vibration and pouring time and offer the possibility of using these concretes in heavily scrapped elements. The incorporation of glass powder and SF as substitutes for cement has, in addition to the above-mentioned benefits, the advantage of reducing the quantity of the admixture while remaining within the range of fluid concretes. This equates to a reduction in the overall cost per m^3 of concrete.

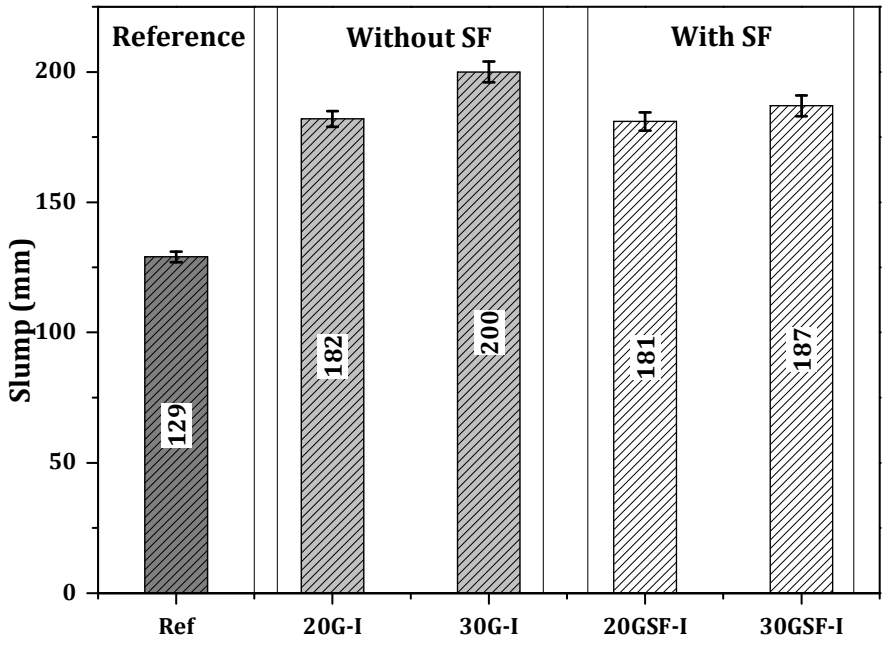

Fig. 5: Workability of the studied concretes.

3.3. Porosity

The results of the water and mercury porosities of concretes at the age of 91 days are shown in Fig. 6. Firstly, the porosity of the control concrete based on CEMI (Ref) is of about 13%, which is in agreement with literature (Issaadi et al., 2017). Furthermore, substitutions of 20% and 30% of cement by glass powder (20G-I and 30G-I) slightly affect the porosity of the concrete. A slight increase of 7.9 and 16.7% was noted in the average porosity of 20G-I and 30G-I, respectively compared to Ref, which corroborates well the findings reported in the literature by (Bouchikhi et al., 2019). This could be due to the fineness of glass powder used which is lower than that of CEM I substituted, especially since the water porosity continues to increase, compared to Ref, with the amount of GP used (20% and 30% of GP). In contrast to what was found for concrete containing only glass powder, the porosity of concretes with 5% of SF decreased according to (Kuzielová et al., 2017). The percentage of diminution was about 19.4 and 20.5% for 20% and 30% of GP, respectively. The decrease is due, on the one hand, to the fineness of SF that is higher than CEMI and GP used, and in the other hand, to the pozzolanic reaction of the mineral addition (SF) with portlandite. In fact, that refines the porosity of

concrete as shown in the literature (Gallé, 2001; Urhan, 1987a). Finally, the difference between water and mercury reflects that water porosimetry can detect a wider range of pores compared to the MIP.

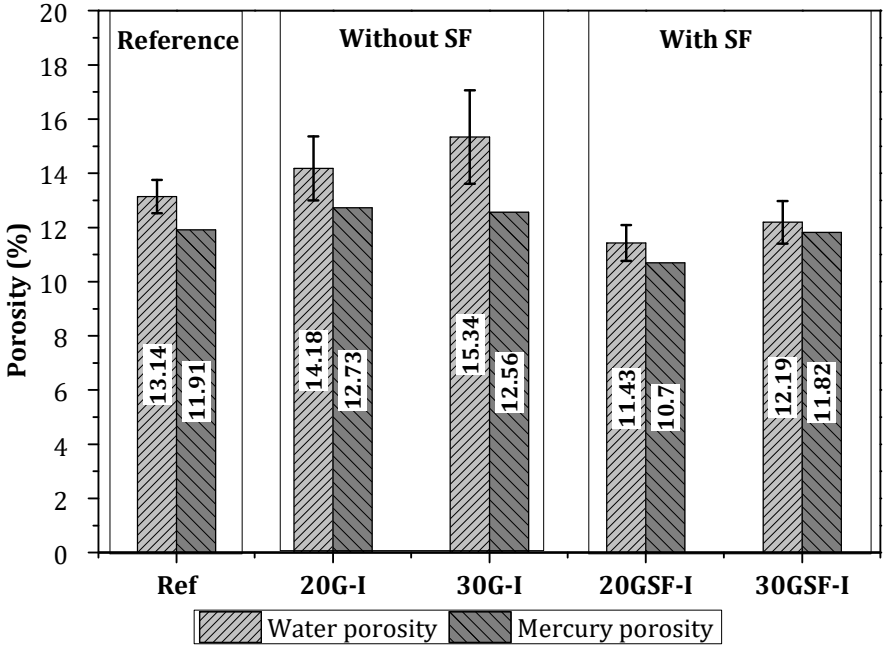

Fig. 6: Water and mercury porosities of studied concretes.

Fig. 7 shows the pore size distribution of concretes obtained by MIP. The pore distributions of Ref, 20G-I and 30G-I are generally monomodal. For 20G-I and 30G-I, we notice the formation of new ranges of micropores (finer than 0.01 µm) and macropores (finer than 100 µm), which confirms the porosity increase for 20G-I and 30G-I compared to the control concrete (Ref). However, the incorporation of 5% of SF highlighted a second range of pores and slowly reduced the critical pore diameter. The decrease confirms the porosity refinement of concretes with glass powder and SF. In general, we note that 30% of glass powder increases the diameter of large pores mainly for 30GSF-I compared to 20GSF-I, with new ranges of pores lower than 0.04 µm and higher than 0.2 µm. These results are in agreement with those for the porosity shown above (Fig. 6).

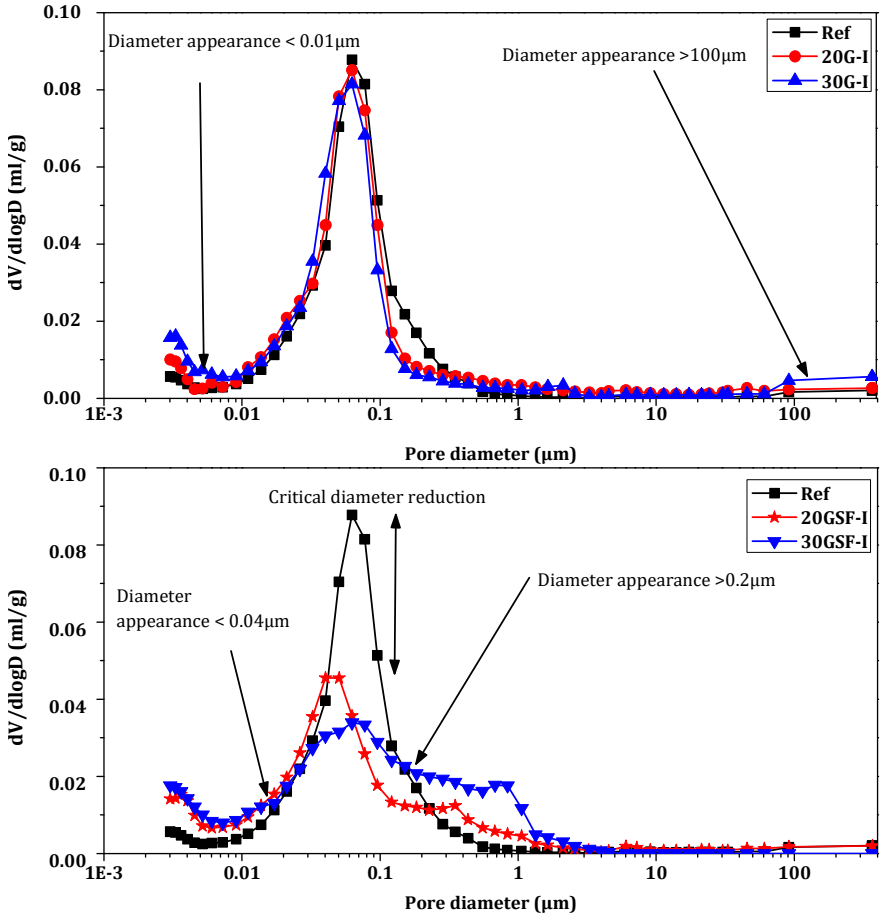

Fig. 7: Pore-size distribution of concretes studied.

3.4. Compressive strength

Fig. 8 shows the compressive strength of the concretes used at the age of 28 and 91 days. The compressive strength for all concretes containing GP is lower than that of the control concrete (Ref), but remains sufficient for structural application (in the range of 36–41 MPa). This is due to a dilution effect which is the immediate consequence of the substitution of a more reactive powder (cement) with a less reactive powder (GP) in the short term (Zidol et al., 2017). Furthermore, the low cementing efficiency of the GP could be due to the low fineness of the GP compared to cement CEMI used (Guo et al., 2020). For Ordinary Portland Cement CEMI, a significant part of the total hydration is done in the short term (28 days) compared to materials with GP. The latter are known for pozzolanic reactions in the long term (more than 91 days).

The control concrete (Ref) reaches its maximal compressive strength of about 57 MPa at 28 days and remains relatively constant with time. However, the compressive strength of the concretes with glass powder continues to increase between 28 and 91 days (+ 5 MPa for 20G-I and 30G-I, and + 10 MPa for 20GSF-I and 30GSF-I). The increase is due to the pozzolanic reaction between portlandite, GP and SF in order to form C-S-H (Idir et al., 2011; Urhan, 1987a, 1987b). This observation is supported by the decrease of the $Ca(OH)_2$ formed after the addition of GP. Further discussions are given in the following sections.

In general, concretes with GP or GP and SF have a satisfactory compressive strength for the structural application. Therefore, GP can be incorporated up to 20% and 30% as a partial replacement of cement in concrete, with a potential benefit in reducing the carbon footprint of these materials.

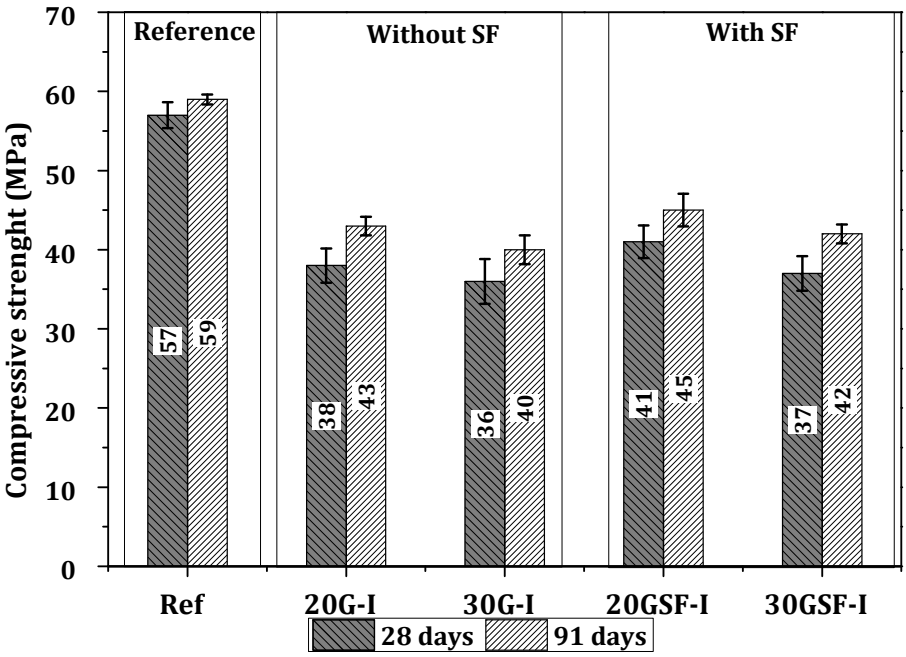

Fig. 8: Compressive strength of the concretes used.

Fig. 9 summarizes the research in the literature studying the effect of GP incorporation in concrete on its compressive strengths at 28 days. The database on compressive strength comprises 10 experimental investigations in the literature (Dyer and Dhir, 2001; Idir et al., 2011; Islam et al., 2017; Khmiri et al., 2013; Matos and Sousa-Coutinho, 2012; Ozkan and Yuksel, 2008; Shayan and Xu, 2006, 2004; Taha and Nounu, 2009; Zidol et al., 2017), with which, in general, our results are in agreement. Furthermore, the mechanical behavior of the concrete in the present study showed a declining trend with the GP replacement ratio. Finally, some exceptions may be observed in some studies where the replacement level was 10%, resulting in the highest resistance of the hardened mixtures.

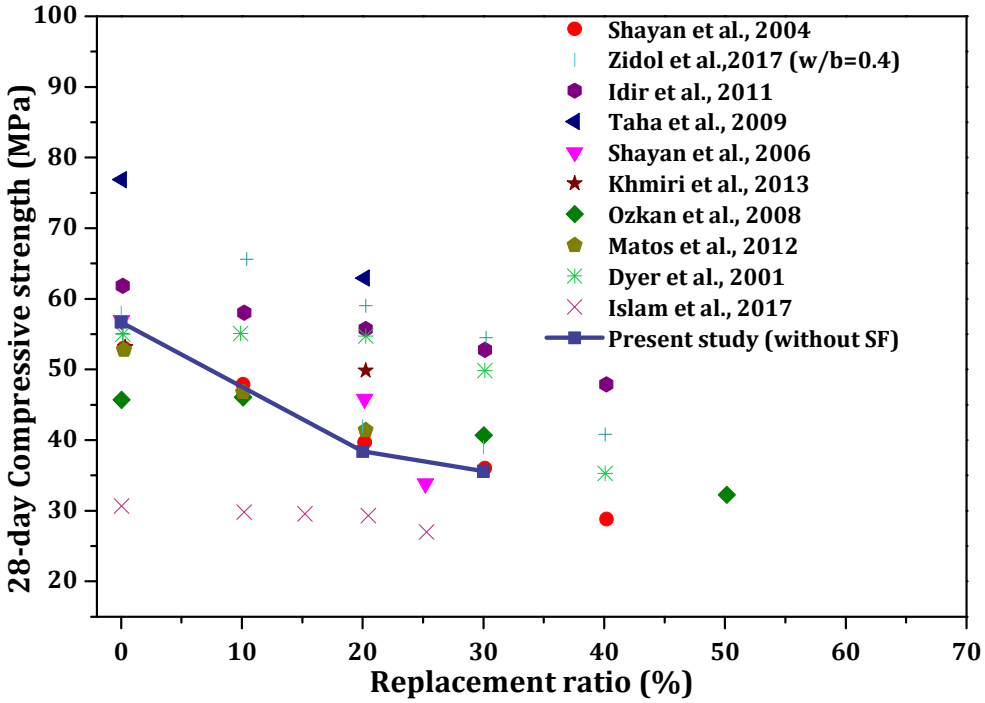

Fig.9: Effect of GP replacement ratio on the 28day compressive strength of mortar and concrete.

3.5. Scanning electron microscopy images (SEM)

SEM images and the corresponding elemental distributions (EDX spectra) given by EDX from EDAX/Gemini (a semi-conductor lithium-doped silicon detector Si:Li) of 30G-I and 30GSF-I are shown in Fig. 10. These analyses show the formation of C-S-H gel and much more in concretes containing SF. In addition, it can be seen on the same images that 30GSF-I (concrete with GP and SF rich in silica as shown in the EDX spectra) has a small volume of voids in the cement matrix compared to 30G-I. Therefore, the SEM images are in accordance with the porosity and pore size distribution results. The SEM observations and EDX analyses show a shortage of portlandite for the 30G-I and 30GSF-I concrete. This decrease is explained by the formation of C-S-H obtained by the pozzolanic reaction between silica and portlandite as shown above (Idir et al., 2011). In fact, this explanation is reinforced by thermogravimetric analyses (TGA) in the section below. In addition, a high formation of C-S-H is observed in 30GS-I concrete compared to 30G-I concrete. This explains the decrease in porosity for concrete containing SF compared to concrete without mineral addition.

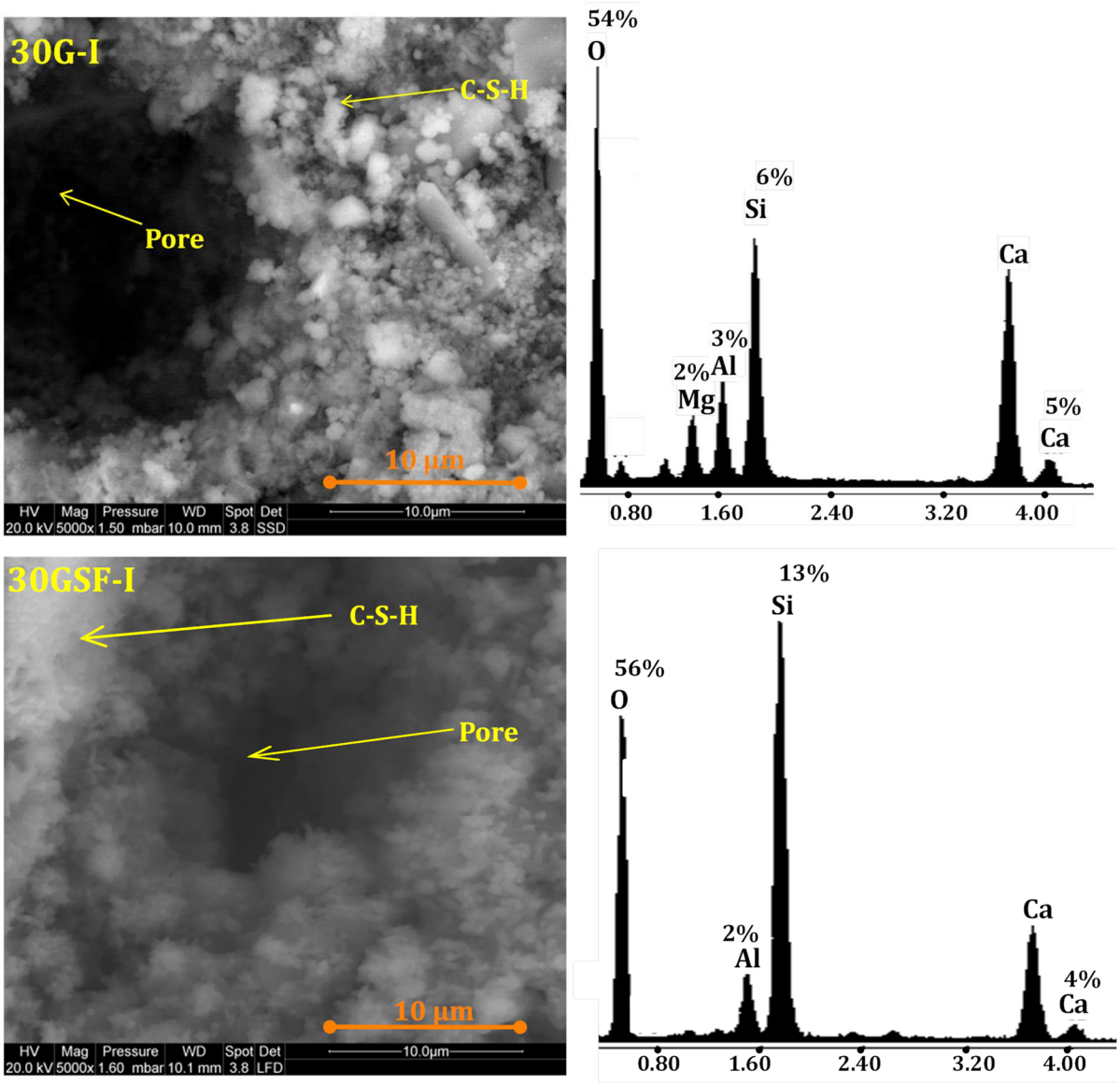

Fig. 10: SEM images and EDX analyses of 30G-I, and 30GSF-I.

3.6. Thermogravimetric analysis (TGA)

TG and derivative TG curves of the concretes studied are presented in Fig. 11. For each dTG curve, the three main phases are mentioned. The first phase at 30°C–145°C corresponds to the free water released from the sample (Issaadi et al., 2015; Loukili et al., 1999). We note a loss of physically bound water of around 3% for Ref, 20G-I, and 30G-I, and 2% of concretes with SF substitution, which requires more water from the pozzolanic reaction (Amar et al., 2017). The second part reflects the release of the chemically bound water from the portlandite. Water loss of 3% for Ref, 2% for 20G-I and 30G- I and about 1% for the other concretes tested was noted. The later concretes have low portlandite content that is consumed by the pozzolanic reaction of GP and SF (Idir et al., 2011; Shi et al., 2005). The third phase corresponds to the $CaCO_3$ decarbonation at 750°C, where we note a high $CaCO_3$ decarbonation for Ref compared to the other concretes, which confirms the high amount of portlandite in Ref without mineral additions or pozzolanic reaction (Amar et al., 2017). The TGA

results are in accordance with the SEM images showing the amount of portlandite in the concretes used with and without SF.

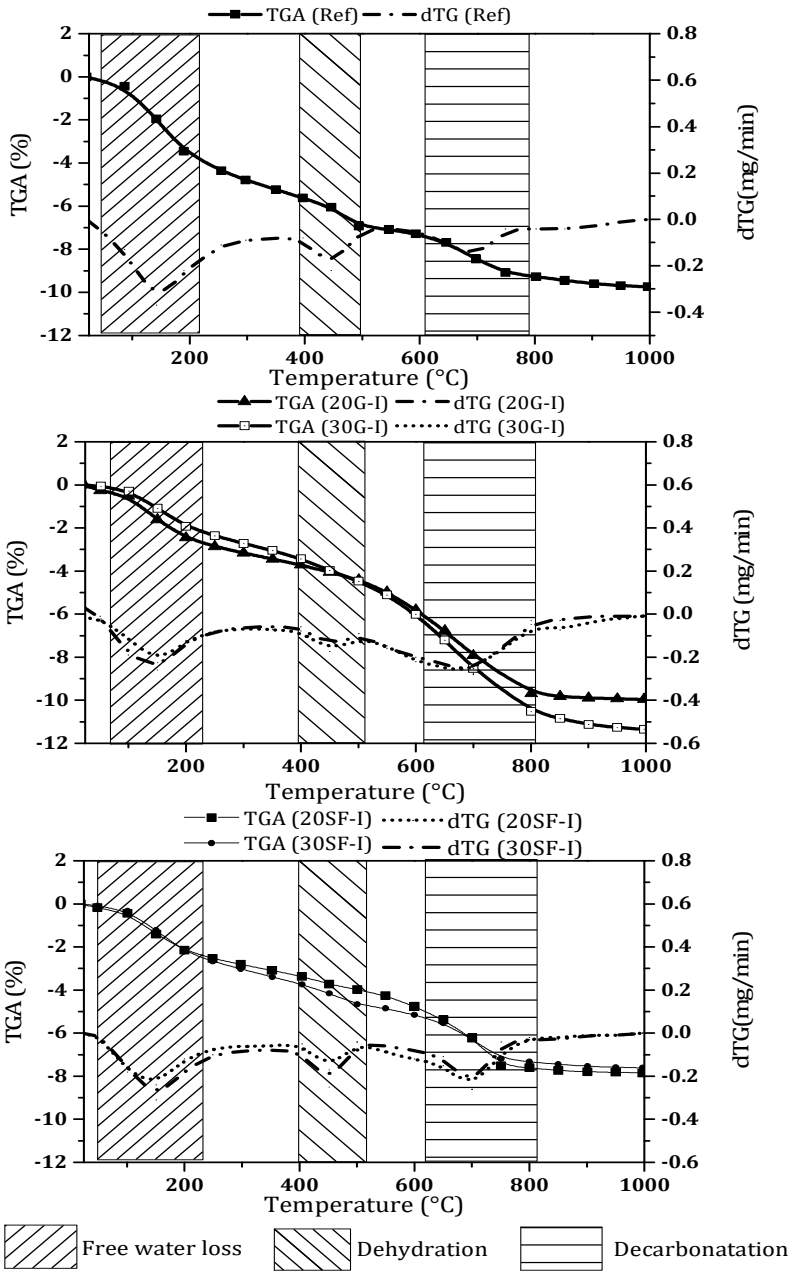

Fig. 11: TG and dTG curves of the studied concretes (solid line: TG; dash line: dTG).

3.7. Specific heat

Figs. 12 and 13 show the specific heat of the concretes obtained by the Calvet® calorimeter. In general, the difference between Ref (highest specific heat obtained) and 30G-I (lowest specific heat) is about 2.3%. The cement mass substitution with 20% and 30% GP decreases the specific heat by about 1.4% for 20GP-I and 2.3% for 30GP-I compared to the control concrete Ref with only CEMI. Despite the porosity changes due to the incorporation of 5% of SF, 20GSF-I and 30GSF-I present a very low increase in the specific heat compared to 20G-I and 30G-I, respectively. For a higher amount of SF

(15%), previous studies showed more effect of SF on the specific heat of concretes (Fu and Chung, 1997; Xu and Chung, 2000). Finally, for all the concretes used, an increase of 13.7% in the specific heat was noted between – 5°C and 40°C (Fig.11).

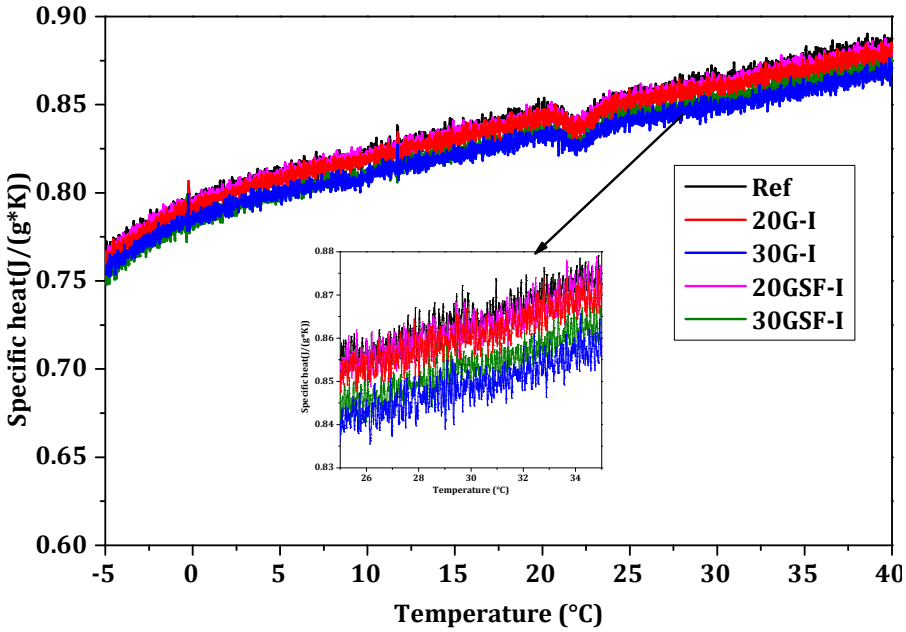

Fig. 12: Specific heat of the studied concretes.

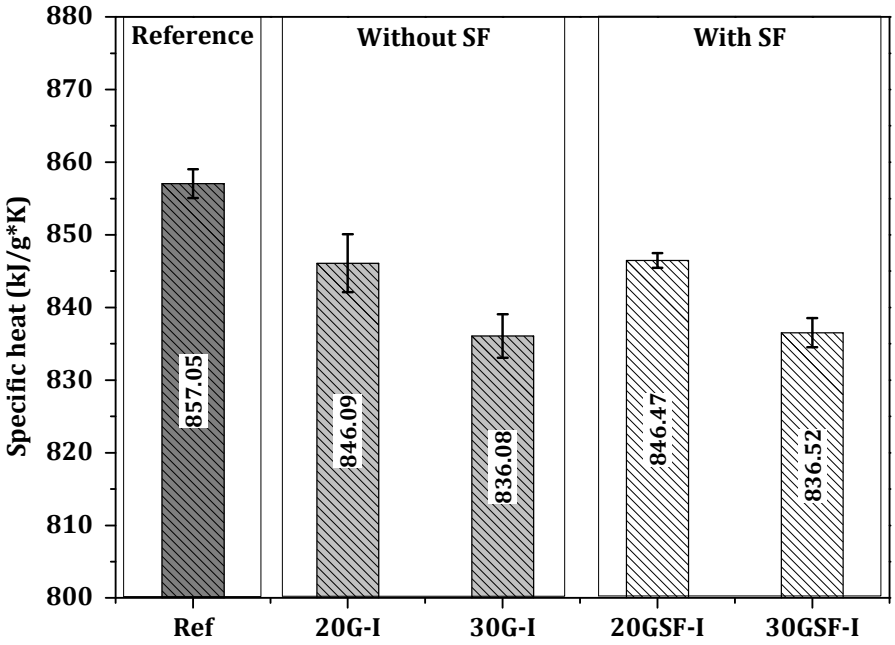

Fig. 13: Specific heat of the concretes used at 23°C.

3.8. Thermal conductivity

Fig. 14 shows the thermal conductivity versus porosity of the tested concretes. Firstly, the cement replacement by 20% and 30% of GP decreases the thermal conductivity of the concretes by 3.7% and 8.9%, respectively. The thermal conductivity reduction is due to the porosity increase for concretes

with GP as shown in Fig. 6. However, the incorporation of SF in concretes decreased their thermal conductivities of about 10% for 20GSF-I and 17% of 30GSF-I, as have been already highlighted by (Fu and Chung, 1997; Xu and Chung, 2000). This is due to the finer particles of SF compared to CEMI and GP whose decrease the total porosities of concrete with SF and changed their pore-size distribution, showing a second range of pore diameters and the appearance of micro and macro pores (see Fig. 7).

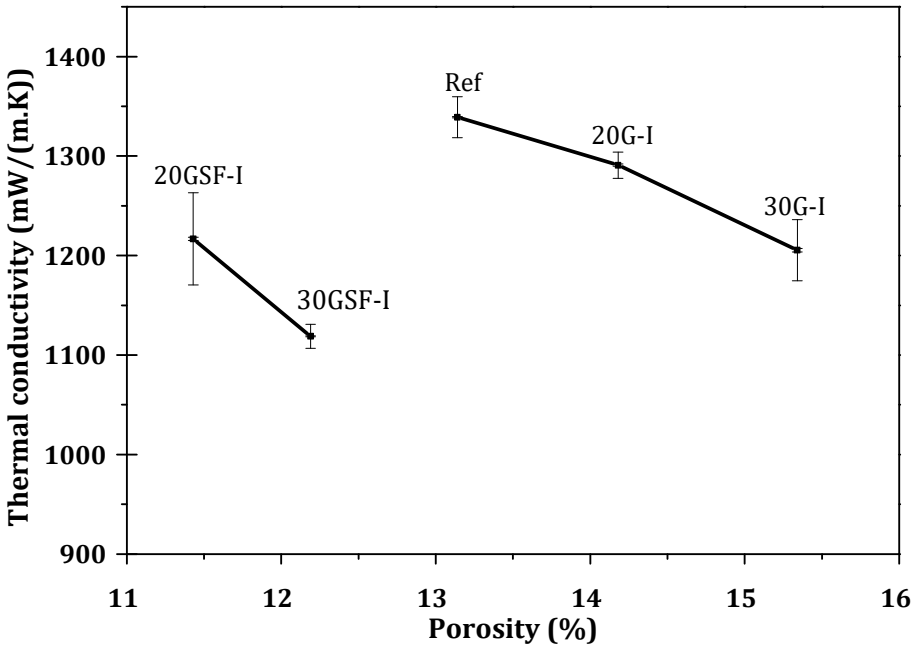

Fig.14: Thermal conductivity of studied concrete.

Fig. 15 shows the thermal conductivity results of the concretes used as a function of their densities. Also, it shows the database in the literature of the thermal conductivities of porous material and the fitting presented by Asadi et al., (2018). The experimental database of the thermal conductivities and densities corresponds to 185 experimental measurements (Bouguerra et al., 1998; Ching and Kaw-Sai, 2010; Demirboğa, 2007; Demirboğa, 2003; Demirboğa and Gül, 2003; Gomes et al., 2017; Johnson Alengaram et al., 2013; Liu et al., 2014; Nguyen et al., 2017; Real et al., 2016; Sayadi et al., 2016; Xu and Chung, 2000). Furthermore, it shows the fitting of the thermal conductivity as a function of the density proposed by the ACI Committee (Demirboga and Kan, 2012). The corresponding empirical functions of the fittings are presented. The results of this study are in accordance with those of the literature performed on different concretes.

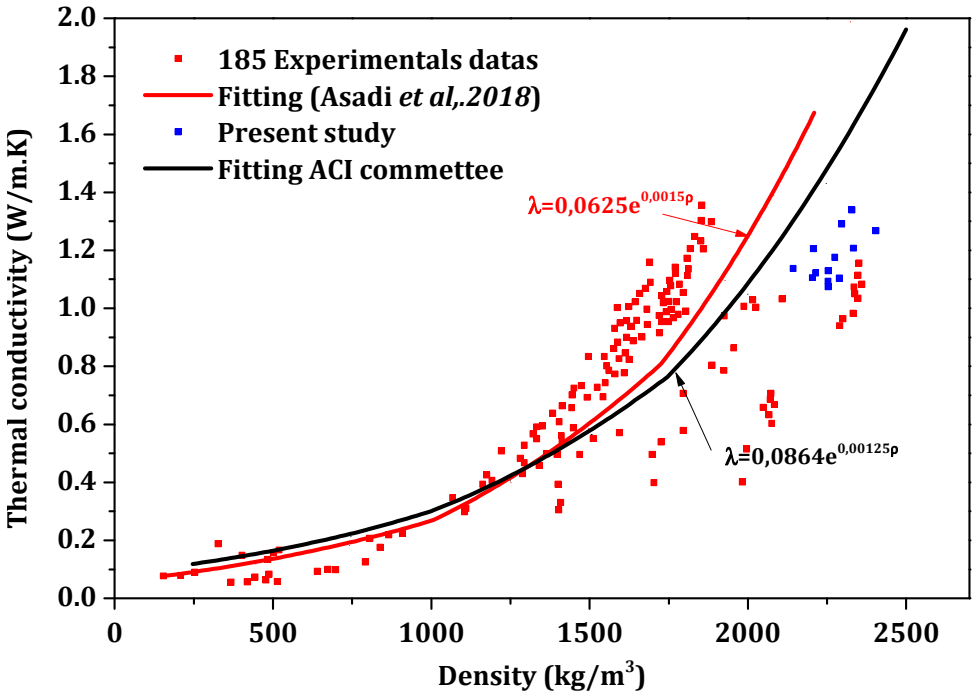

Fig. 15: The thermal conductivity of concretes as a function of density

3.9. Sorption isotherm

Fig. 16 shows the average sorption isotherms of the concretes used and the standard deviation for three measurements at the age of 91 days. It highlights the effect of the GP and SF on the water vapor diffusion and the sorption isotherms. Firstly, we observed an increase of the hysteresis area with the replacement of cement by GP and SF. The latter changes the concrete microstructure and the pore-size distribution. We note that the sorption capacity of all the studied concretes is almost the same in the super-hygroscopic zone. The sorption isotherms exhibit hysteresis between the sorption phase and the desorption phase over the entire moisture range. The effect of hysteresis is not fully understood, but it is generally assumed that the moisture content at the top equilibrium for desorption is due to the entrapment of water within large pores surrounded by small pores, known as the "ink bottle effect" (Ishida et al., 2007). In fact, the hysteresis is due to the changes in the contact angle between the adsorbed water and the internal surface of the material. During the drying cycle, the water coating that exists on the surface of the internal capillary micro-pores is in contact with an already fully moist surface, while during the humidification cycle the water film formed is in contact with a dry and not yet wet surface (C.M. Chen and Wangaard, 1968).

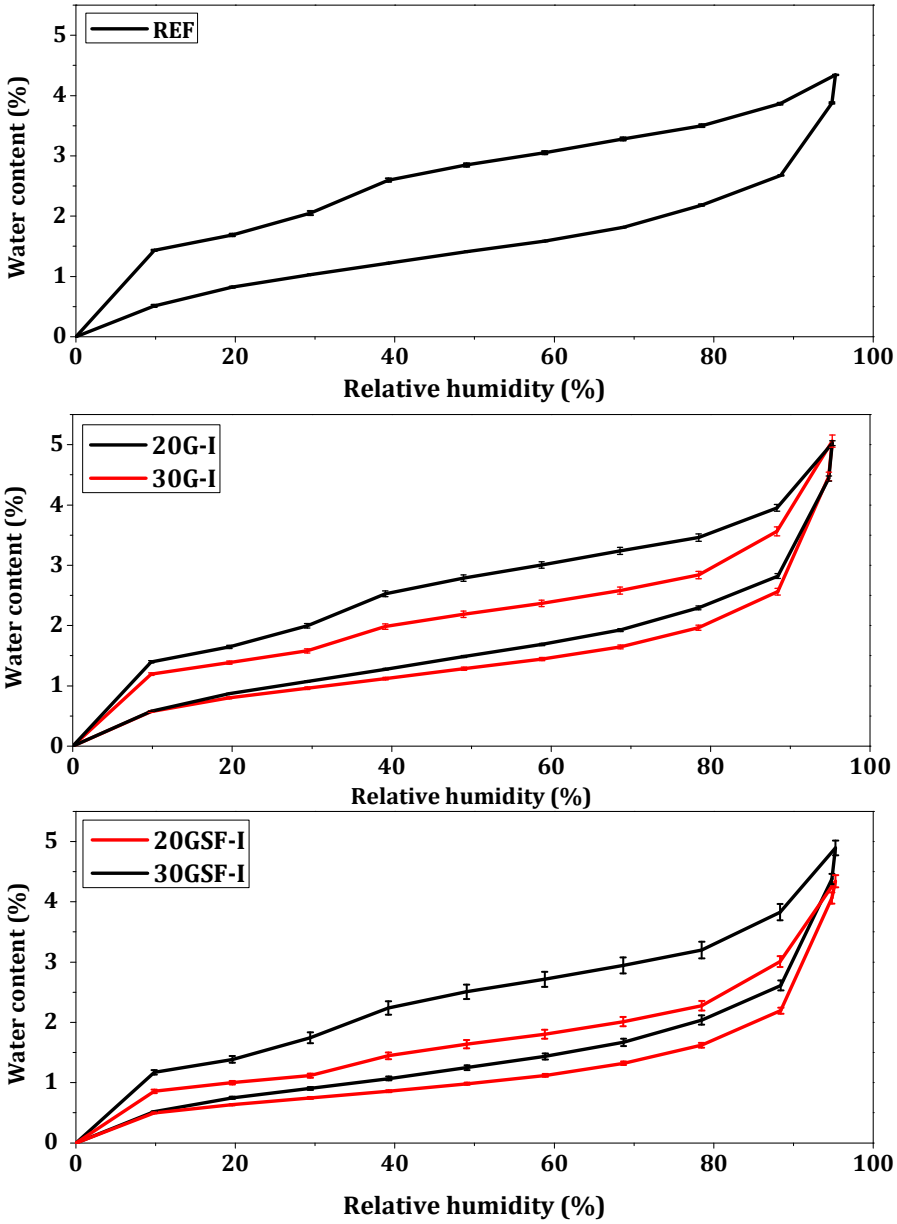

Fig. 16: Sorption isotherms of the studied concretes.

In order to study the effect of the incorporation of GP and SF in concretes on the moisture storage capacity, the latter was deduced from the sorption isotherms for each concrete. This represents the ability of the material to adsorb and release moisture. The moisture storage capacity (called C_m) is often used for hydric transfer modeling. The C_m curves are shown in Fig. 1. For high humidity (>80%), the incorporation of GP in concretes increases their moisture storage capacity compared to the control concrete (Ref). This is attributed to the effect of porosity on this intrinsic mass transfer parameter. On the one hand, because the GP is less permeable, it slows down the diffusivity and storage of moisture. On the other hand, given the angular shape of the glass powder, it introduces small ITZ, in which the pozzolanic reaction between the glass rich in SiO_2 and the portlandite $Ca(OH)_2$ takes a long time to form the C-S-H that clogs the porosity (Bouchikhi et al., 2019; Idir et al., 2011).

In general, the storage capacity of humidity varies according to the relative humidity (RH). For RH ranging from 10% to 80%, the C_m value is low and remains constant. Then, it significantly decreases for the hygroscopic zones (RH > 80%). This variation is due to the type of sorption–desorption isotherm (type II according to the IUPAC classification (Sing KS., 1985)).

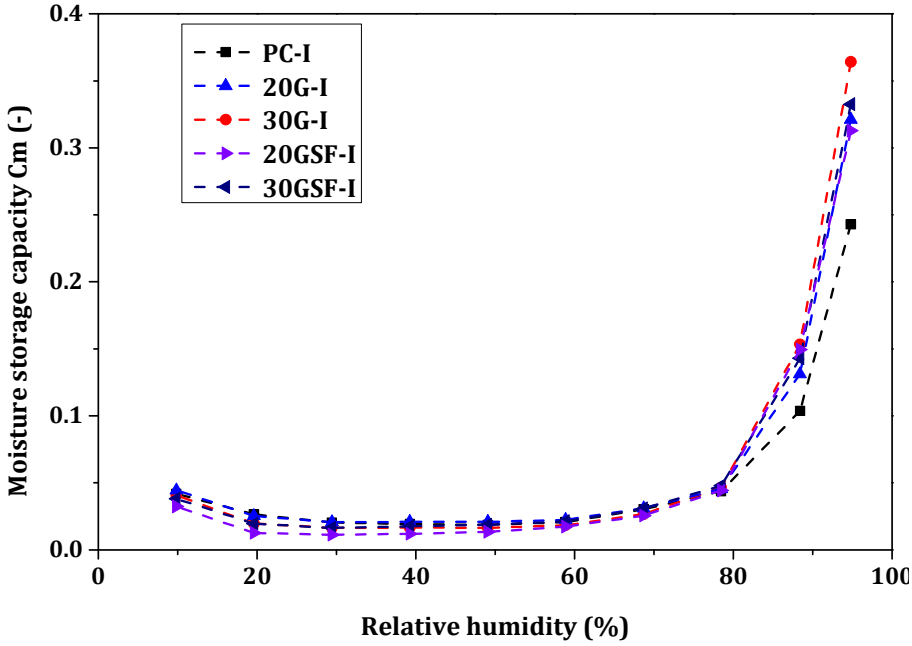

Fig. 17: Moisture storage capacity of the concretes studied.

3.10. Water vapor permeability

The water vapor permeability of the concretes used is shown in Fig. 18, using the wet cup method. The results highlight a significant increase in water vapor permeability with the replacement of cement by GP and SF. This is explained by the changes of the concrete microstructure as shown above (porosity, pore size distribution and possible tortuosity and constrictivity) due to the tion of the binder (cement + GP) and the pozzolanic reaction of the GP. However, the use of SF in concretes increased the water vapor permeability, although it is assumed to reduce the concrete porosity. In fact, SF reduces the total porosity and the pore diameter of the concrete and increases its tortuosity (Omran and Tagnit-Hamou, 2016). The latter could affect the water vapor permeability of concretes with GP and SF compared to Ref.

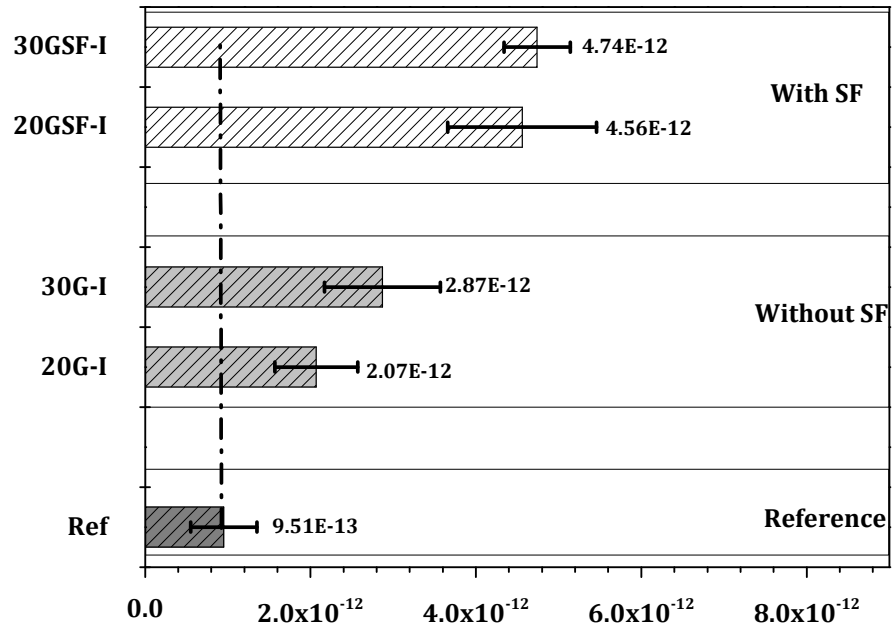

Fig. 18: Water vapor permeability of the used concretes in [kg/m.s.Pa].

4. Conclusion

An experimental study was carried out on the effect of the partial mass replacement of cement by glass powder and silica fume in concretes. The objective was to assess the hygrothermal properties of the concrete and the impact of its microstructure. The results obtained for the concrete tested are satisfactory, making it a good material for building and construction. The following conclusions can be drawn:

- Due to its fineness, the GP used increases the concrete's consistency up to 55% and the porosity up to 20%.
- Despite the use of 5% of SF, the incorporation of the used GP in concrete decreases its compressive strength at 28 and 91 days compared to the control concrete with CEMI, but remains sufficient for structural applications.
- The incorporation of 20% and 30% of GP in concrete reduces it heat capacity by 1.4% and 2.3%, respectively compared to control concrete. However, the addition of 5% SF shows slightly effects on heat capacity.
- Cement replacement by 20 or 30% GP and 5% SF significantly decreases the thermal conductivity of the concrete due to the microstructure changes.
- Finally, the replacement of cement by GP (20% and 30%) and SF (5%) in concrete increases its moisture storage capacity (C_m) for the super-hygrothermal zones as well as its water vapor permeability (up to 5 times for 30GSF-I compared to the control concrete).

The experimental characterization campaign reported in this work has not only enriched the database of concrete properties but has also supplied the numerical simulation model with reliable input data to predict their hygrothermal behavior. Therefore, further numerical investigation will be achieved to

highlight the advantages of using these materials in terms of energy performance, durability and the environmental impacts.

Acknowledgements

The Region and the European Union support the project < CPER BATIMENT DURABLE. Axis 2 MADUR Project: High-performance building materials with low environmental impact, sustainable and resilient > within the framework of the « Operational Program FEDER/FSE 2014-2020 » and Energy saving certificate program of the Ministry of Ecological and Solidarity Transition 'SmartReno support" 2019-2021. We acknowledge support from the microscopies platform of LaSIE for the realization of SEM observations.

References

AFPC-AFREM, 2007. Durabilité des bétons : Méthodes recommandées pour la mesure des grandeurs associées à la durabilité.

Aliabdo, A.A., Abd Elmoaty, A.E.M., Aboshama, A.Y., 2016. Utilization of waste glass powder in the production of cement and concrete. Constr. Build. Mater. 124, 866–877. https://doi.org/10.1016/j.conbuildmat.2016.08.016

Amar, M., Benzerzour, M., Abriak, N., Mamindy-pajany, Y., 2017. Study of the pozzolanic activity of a dredged sediment from Dunkirk harbour. Powder Technol. https://doi.org/10.1016/j.powtec.2017.07.055

Antoni, Chandra, L., Hardjito, D., 2015. The Impact of Using Fly Ash, Silica Fume and Calcium Carbonate on the Workability and Compressive Strength of Mortar. Procedia Eng. 125, 773–779. https://doi.org/10.1016/j.proeng.2015.11.132

Asadi, I., Shafigh, P., Bin, Z.F., Hassan, A., Mahyuddin, N.B., 2018. Thermal conductivity of concrete - A review Reference. J. Build. Eng. https://doi.org/10.1016/j.jobe.2018.07.002

ASTM C1702, 2017. Standard Test Method for Measurement of Heat of Hydration of Hydraulic Cementitious Materials Using Isothermal Conduction Calorimetry.

ASTM D4404–84, 1998. Standard Test Method for Determination of Pore Volume and Pore Volume Distribution of Soil and Rock by Mercury Intrusion Porosimetry.

Bani Ardalan, R., Joshaghani, A., Hooton, R.D., 2017. Workability retention and compressive strength of self-compacting concrete incorporating pumice powder and silica fume. Constr. Build. Mater. 134, 116–122. https://doi.org/10.1016/j.conbuildmat.2016.12.090

Bentz, D.P., Peltz, M.A., 2011. Thermal properties of high-volume fly ash mortars and concretes. https://doi.org/10.1177/1744259110376613

563 Berenguer, R.A., Capraro, A.P.B., de Medeiros, M.H.F., Carneiro, A.M.P., De Oliveira, R.A., 2020.
564 Sugar cane bagasse ash as a partial substitute of Portland cement: Effect on mechanical
565 properties and emission of carbon dioxide. J. Environ. Chem. Eng. 8, 103655.
566 https://doi.org/10.1016/j.jece.2020.103655

567 Bisht, K., Ramana, P. V., 2018. Sustainable production of concrete containing discarded beverage
568 glass as fine aggregate. Constr. Build. Mater. 177, 116–124.
569 https://doi.org/10.1016/j.conbuildmat.2018.05.119

570 Bouchikhi, A., Benzerzour, M., Abriak, N., Maherzi, W., Mamindy-pajany, Y., 2019. Study of the
571 impact of waste glasses types on pozzolanic activity of cementitious matrix. Constr. Build.
572 Mater. 197, 626–640. https://doi.org/10.1016/j.conbuildmat.2018.11.180

573 Bouguerra, A., Ledhem, A., de Barquin, F., Dheilly, R.M., Quéneudec, M., 1998. Effect of
574 microstructure on the mechanical and thermal properties of lightweight concrete prepared from
575 clay, cement, and wood aggregates. Cem. Concr. Res. 28, 1179–1190.
576 https://doi.org/10.1016/S0008-8846(98)00075-1

577 Bueno, E.T., Paris, J.M., Clavier, K.A., Spreadbury, C., Ferraro, C.C., Townsend, T.G., 2020. A
578 review of ground waste glass as a supplementary cementitious material: A focus on alkali-silica
579 reaction. J. Clean. Prod. 257, 120180. https://doi.org/10.1016/j.jclepro.2020.120180

580 C.M. Chen, Wangaard, F.F., 1968. Wettability and the hysteresis effect in the sorption of water vapor
581 by wood. Wood Sci. Technol. 2, 177–178.

582 Chand, G., Happy, S.K., Ram, S., 2021. Assessment of the properties of sustainable concrete produced
583 from quaternary blend of portland cement, glass powder, metakaolin and silica fume. Clean. Eng.
584 Technol. 4, 100179. https://doi.org/10.1016/j.clet.2021.100179

585 Chandra Paul, S., Šavija, B., Babafemi, A.J., 2018. A comprehensive review on mechanical and
586 durability properties of cement-based materials containing waste recycled glass. J. Clean. Prod.
587 198, 891–906. https://doi.org/10.1016/j.jclepro.2018.07.095

588 Cherif, R., Hamami, A.E.A., Aït-Mokhtar, A., 2020. Effects of leaching and chloride migration on the
589 microstructure and pore solution of blended cement pastes during a migration test. Constr. Build.
590 Mater. 240, 117934. https://doi.org/10.1016/j.conbuildmat.2019.117934

591 Ching, N., Kaw-Sai, L., 2010. Thermal conductivity of newspaper sandwiched aerated lightweight
592 concrete panel. Energy Build. 42, 2452–2456. https://doi.org/10.1016/j.enbuild.2010.08.026

593 Conforto, E., Joguet, N., Buisson, P., Vendeville, J., Chaigneau, C., Maugard, T., 2015. An optimized
594 methodology to analyze biopolymer capsules by environmental scanning electron microscopy.
595 Mater. Sci. Eng. C 47, 357–366. https://doi.org/10.1016/j.msec.2014.11.054

De Castro, S., De Brito, J., 2013. Evaluation of the durability of concrete made with crushed glass aggregates. J. Clean. Prod. 41, 7–14. https://doi.org/10.1016/j.jclepro.2012.09.021

Demirboğa, R., 2007. Thermal conductivity and compressive strength of concrete incorporation with mineral admixtures. Build. Environ. 42, 2467–2471. https://doi.org/10.1016/j.buildenv.2006.06.010

Demirboğa, R., 2007. Thermal conductivity and compressive strength of concrete incorporation with mineral admixtures. Build. Environ. 42, 2467–2471. https://doi.org/10.1016/j.buildenv.2006.06.010

Demirboğa, R., 2003. Influence of mineral admixtures on thermal conductivity and compressive strength of mortar. Energy Build. 35, 189–192. https://doi.org/https://doi.org/10.1016/S0378-7788(02)00052-X

Demirboğa, R., Gül, R., 2003. Thermal conductivity and compressive strength of expanded perlite aggregate concrete with mineral admixtures. Energy Build. 35, 1155–1159. https://doi.org/https://doi.org/10.1016/j.enbuild.2003.09.002

Demirboga, R., Kan, A., 2012. Thermal conductivity and shrinkage properties of modified waste polystyrene aggregate concretes. Constr. Build. Mater. 35, 730–734. https://doi.org/10.1016/j.conbuildmat.2012.04.105

Du, Y., Yang, W., Ge, Y., Wang, S., Liu, P., 2021. Thermal conductivity of cement paste containing waste glass powder, metakaolin and limestone filler as supplementary cementitious material. J. Clean. Prod. 287, 125018. https://doi.org/10.1016/j.jclepro.2020.125018

Dyer, T.D., Dhir, R.K., 2001. Chemical Reactions of Glass Cullet Used as Cement Component. J. Mater. Civ. Eng. 13, 412–417. https://doi.org/10.1061/(ASCE)0899-1561(2001)13:6(412)

EN 12390-3, 2019. Essais pour béton durci - Partie 3 : résistance à la compression des éprouvettes.

EN 12664, 2001. Performance thermique des matériaux et produits pour le bâtiment - Détermination de la résistance thermique par la méthode de la plaque chaude gardée et la méthode fluxmétrique - Produits secs et humides de moyenne et basse résistance thermiqu.

EN 12667, 2001. Performance thermique des matériaux et produits pour le bâtiment - Détermination de la résistance thermique par la méthode de la plaque chaude gardée et la méthode fluxmétrique - Produits de haute et moyenne résistance thermique,».

EN 13263-1, 2005. Fumée de silice pour béton - Partie 1 : définitions, exigences et critères de conformité.

EN 197-1, 2012. Ciment - Partie 1 : composition, spécifications et critères de conformité des ciments

courants [WWW Document].

Federico, L.M., Chidiac, S.E., 2009. Waste glass as a supplementary cementitious material in concrete – Critical review of treatment methods. Cem. Concr. Compos. 31, 606–610. https://doi.org/10.1016/j.cemconcomp.2009.02.001

Feldman, R.F., 1981. Pore Structure Formation during Hydration of Fly Ash and Slag Cement Blends. Mater. Res. Soc. Pittsburgh, PA 124–133.

Fu, X., Chung, D.D.L., 1997. Effects of silica fume, latex, methylcellulose, and carbon fibers on the thermal conductivity and specific heat of cement paste. Cem. Concr. Res. 27, 1799–1804. https://doi.org/10.1016/S0008-8846(97)00174-9

Gallé, C., 2001. Effect of drying on cement-based materials pore structure as identified by mercury intrusion porosimetry - A comparative study between oven-, vacuum-, and freeze-drying. Cem. Concr. Res. 31, 1467–1477. https://doi.org/10.1016/S0008-8846(01)00594-4

Gencel, O., Karadag, O., Oren, O.H., Bilir, T., 2021. Steel slag and its applications in cement and concrete technology: A review. Constr. Build. Mater. 283, 122783. https://doi.org/10.1016/j.conbuildmat.2021.122783

Gerges, N.N., Issa, C.A., Fawaz, S.A., Jabbour, J., Jreige, J., 2018. Recycled Glass Concrete : Coarse and Fine Aggregates. EJERS, Eur. J. Eng. Res. Sci. 3, 1–9. https://doi.org/http://dx.doi.org/10.24018/ejers.2018.3.1.533

Gökçe, H.S., Hatungimana, D., Ramyar, K., 2019. Effect of fly ash and silica fume on hardened properties of foam concrete 194, 1–11. https://doi.org/10.1016/j.conbuildmat.2018.11.036

Gomes, M.G., Manga, L.M., Soares, A., Brito, J. De, 2017. The influence of moisture content on the thermal conductivity of external thermal mortars. Constr. Build. Mater. 135, 279–286. https://doi.org/10.1016/j.conbuildmat.2016.12.166

Guo, P., Meng, W., Nassif, H., Gou, H., Bao, Y., 2020. New perspectives on recycling waste glass in manufacturing concrete for sustainable civil infrastructure. Constr. Build. Mater. 257, 119579. https://doi.org/10.1016/j.conbuildmat.2020.119579

Hussain, S.E. and R., 1994. Corrosion Resistance Performance of Fly Ash Blended Cement Concrete. ACI Mater. J. 91, 264–272.

Idir, R., Cyr, M., Tagnit-Hamou, A., 2011. Pozzolanic properties of fine and coarse color-mixed glass cullet. Cem. Concr. Compos. 33, 19–29. https://doi.org/10.1016/j.cemconcomp.2010.09.013

Idir, R., Cyr, M., Tagnit-Hamou, A., 2010. Use of fine glass as ASR inhibitor in glass aggregate mortars. Constr. Build. Mater. 24, 1309–1312.

https://doi.org/10.1016/j.conbuildmat.2009.12.030

Ishida, T., Maekawa, K., Kishi, T., 2007. Enhanced modeling of moisture equilibrium and transport in cementitious materials under arbitrary temperature and relative humidity history 37, 565–578. https://doi.org/10.1016/j.cemconres.2006.11.015

Islam, G.M.S., Rahman, M.H., Kazi, N., 2017. Waste glass powder as partial replacement of cement for sustainable concrete practice. Int. J. Sustain. Built Environ. 6, 37–44. https://doi.org/10.1016/j.ijsbe.2016.10.005

ISO 12571, 2000. Performance hygrothermique des matériaux et produits pour le bâtiment, Détermination des propriétés de sorption hygroscopique.

ISO 12572, 2001. Performance hygrothermique des matériaux et produits pour le bâtiment, Détermination des propriétés de transmission de la vapeur d'eau.

Issaadi, N., Hamami, A.A., Belarbi, R., Aït-Mokhtar, A., 2017. Experimental assessment of the spatial variability of porosity, permeability and sorption isotherms in an ordinary building concrete. Heat Mass Transf. und Stoffuebertragung 53, 3037–3048. https://doi.org/10.1007/s00231-017-2041-4

Issaadi, N., Nouviaire, A., Belarbi, R., Aït-Mokhtar, A., 2015. Moisture characterization of cementitious material properties: Assessment of water vapor sorption isotherm and permeability variation with ages. Constr. Build. Mater. 83, 237–247. https://doi.org/10.1016/j.conbuildmat.2015.03.030

Johnson Alengaram, U., Al Muhit, B.A., bin Jumaat, M.Z., Jing, M.L.Y., 2013. A comparison of the thermal conductivity of oil palm shell foamed concrete with conventional materials. Mater. Des. 51, 522–529. https://doi.org/10.1016/j.matdes.2013.04.078

Khmiri, A., Chaabouni, M., Samet, B., 2013. Chemical behaviour of ground waste glass when used as partial cement replacement in mortars. Constr. Build. Mater. 44, 74–80. https://doi.org/10.1016/j.conbuildmat.2013.02.040

Khokhar, M.I.A., Roziere, E., Turcry, P., Grondin, F., Loukili, A., 2010. Mix design of concrete with high content of mineral additions: Optimisation to improve early age strength. Cem. Concr. Compos. 32, 377–385. https://doi.org/10.1016/j.cemconcomp.2010.01.006

Kuzielová, E., Žemlička, M., Bartoničková, E., Palou, M.T., 2017. The correlation between porosity and mechanical properties of multicomponent systems consisting of Portland cement–slag–silica fume–metakaolin. Constr. Build. Mater. 135, 306–314. https://doi.org/10.1016/j.conbuildmat.2016.12.105

692 Liu, M.Y.J., Alengaram, U.J., Jumaat, M.Z., Mo, K.H., 2014. Evaluation of thermal conductivity,
693 mechanical and transport properties of lightweight aggregate foamed geopolymer concrete.
694 Energy Build. 72, 238–245. https://doi.org/10.1016/j.enbuild.2013.12.029

695 Loukili, A., Khelidj, A., Richard, P., 1999. Hydration kinetics, change of relative humidity, and
696 autogenous shrinkage of ultra-high-strength concrete. Cem. Concr. Res. 29, 577–584.
697 https://doi.org/10.1016/S0008-8846(99)00022-8

698 Manmohan, D. and Metha, P.K., 1981. Influence of Pozzolanic, Slag and Chemical Admixtures on
699 Pore Size Distribution and Permeability of Hardened Cement Pastes. Cement Concrete and
700 Aggregates, 3, 63–67.

701 Matos, A.M., Sousa-Coutinho, J., 2012. Durability of mortar using waste glass powder as cement
702 replacement. Constr. Build. Mater. 36, 205–215.
703 https://doi.org/10.1016/j.conbuildmat.2012.04.027

704 Meyer, C., Egosi, N., Andela, C., 2001. Concrete with waste glass as aggregate. J. Chem. Inf. Model.
705 53, 1689–1699. https://doi.org/10.1017/CBO9781107415324.004

706 Miller, S.A., Horvath, A., Monteiro, P.J.M., 2016. Readily implementable techniques can cut annual
707 CO 2 emissions from the production of concrete by over 20%. Environ. Res. Lett. 11, 074029.
708 https://doi.org/10.1088/1748-9326/11/7/074029

709 Mohajerani, A., Vajna, J., Cheung, T.H.H., Kurmus, H., Arulrajah, A., Horpibulsuk, S., 2017.
710 Practical recycling applications of crushed waste glass in construction materials: A review.
711 Constr. Build. Mater. 156, 443–467. https://doi.org/10.1016/j.conbuildmat.2017.09.005

712 NF EN 12350-2, 2012. Essais pour béton frais - Partie 2 : essai d'affaissement, Avril 2012.

713 NF EN 206, 2016. Béton - Spécification, performance, production et conformité - Complément
714 national à la norme NF EN 206.

715 NF EN 821-3, 2005. Céramiques techniques avancées - Céramiques monolithiques - Propriétés
716 thermophysiques - Partie 3 : détermination de la chaleur spécifique, Juin 2005.

717 NF EN 933-1, 2012. Essais pour déterminer les caractéristiques géométriques des granulats - Partie 1 :
718 détermination de la granularité - Analyse granulométrique par tamisage.

719 NF EN ISO 18757, 2006. Céramiques techniques - Détermination de la surface spécifique (aire
720 massique) des poudres céramiques par adsorption de gaz à l'aide de la méthode BET.

721 Nguyen, L.H., Beaucour, A.-L., Ortola, S., Noumowé, A., 2017. Experimental study on the thermal
722 properties of lightweight aggregate concretes at different moisture contents and ambient
723 temperatures. Constr. Build. Mater. 151, 720–731.

https://doi.org/10.1016/j.conbuildmat.2017.06.087

Oliveira, R., De Brito, J., Veiga, R., 2015. Reduction of the cement content in rendering mortars with fine glass aggregates. J. Clean. Prod. 95, 75–88. https://doi.org/10.1016/j.jclepro.2015.02.049

Omran, A., Tagnit-Hamou, A., 2016. Performance of glass-powder concrete in field applications. Constr. Build. Mater. 109, 84–95. https://doi.org/10.1016/j.conbuildmat.2016.02.006

Ozkan, O., Yuksel, I., 2008. Studies on mortars containing waste bottle glass and industrial by-products. Constr. Build. Mater 22, 1288–1298. https://doi.org/10.1016/j.conbuildmat.2007.01.015

Penacho, P., De Brito, J., Rosário Veiga, M., 2014. Physico-mechanical and performance characterization of mortars incorporating fine glass waste aggregate. Cem. Concr. Compos. 50, 47–59. https://doi.org/10.1016/j.cemconcomp.2014.02.007

Perraton, D., Aitcin, P., Vezina, D., 1988. Permeabilities of silica fume concrete. Am. Concr. Institue 108, 63–84.

Rahman, M.H., 2015. A Study on Potential of Recycled Glass as Cementitious Material in Concrete. Louisiana State University. https://doi.org/DOI: 10.13140/RG.2.1.2956.7602

Raju, A.S., Anand, K.B., Rakesh, P., 2020. Partial replacement of Ordinary Portland cement by LCD glass powder in concrete. Mater. Today Proc. https://doi.org/10.1016/j.matpr.2020.10.661

Rashad, A.M., 2015. Recycled cathode ray tube and liquid crystal display glass as fine aggregate replacement in cementitious materials. Constr. Build. Mater. 93, 1236–1248. https://doi.org/10.1016/j.conbuildmat.2015.05.004

Rashad, A.M., 2014. Recycled waste glass as fine aggregate replacement in cementitious materials based on Portland cement. Constr. Build. Mater. 72, 340–357. https://doi.org/10.1016/j.conbuildmat.2014.08.092

Real, S., Bogas, J.A., Gomes, M. da G., Ferrer, B., 2016. Thermal conductivity of structural lightweight aggregate concrete. Mag. Concr. Res. 68, 798–808. https://doi.org/10.1680/jmacr.15.00424

Samtur, H.R., 1974. Glass Recycling and Reuse. Report 17, University of Wisconsin, Madison Institute for Environmental Studies.

Santos, T., Gomes, M.I., Silva, A.S., Ferraz, E., Faria, P., 2020. Comparison of mineralogical, mechanical and hygroscopic characteristic of earthen, gypsum and cement-based plasters. Constr. Build. Mater. 254, 119222. https://doi.org/10.1016/j.conbuildmat.2020.119222

Sayadi, A.A., Tapia, J. V, Neitzert, T.R., Clifton, G.C., 2016. Effects of expanded polystyrene (EPS) particles on fire resistance , thermal conductivity and compressive strength of foamed concrete. Constr. Build. Mater. 112, 716–724. https://doi.org/10.1016/j.conbuildmat.2016.02.218

Sellevold, T., Bager, E.., Klitgaard, D.., Jensen, E., Knudsen, T., 1982. Silica Fume Cement Paste—Hydration and Pore Structure. Condensed Silica Fume in Concrete.

Serpa, D., Santos Silva, A., De Brito, J., Pontes, J., Soares, D., 2013. ASR of mortars containing glass. Constr. Build. Mater. 47, 489–495. https://doi.org/10.1016/j.conbuildmat.2013.05.058

Shao, Y., Lefort, T., Moras, S., Rodriguez, D., 2000. Studies on concrete containing ground waste glass. Cem. Concr. Res. 30, 91–100. https://doi.org/10.1016/S0008-8846(99)00213-6

Shayan, A., Xu, A., 2006. Performance of glass powder as a pozzolanic material in concrete: A field trial on concrete slabs. Cem. Concr. Res. 36, 457–468. https://doi.org/10.1016/j.cemconres.2005.12.012

Shayan, A., Xu, A., 2004. Value-added utilisation of waste glass in concrete. Cem. Concr. Res. 34, 81–89. https://doi.org/10.1016/S0008-8846(03)00251-5

Shen, D., Jiao, Y., Kang, J., Feng, Z., Shen, Y., 2020. Influence of ground granulated blast furnace slag on early-age cracking potential of internally cured high performance concrete. Constr. Build. Mater. 233, 117083. https://doi.org/10.1016/j.conbuildmat.2019.117083

Shi, C., Wu, Y., Riefler, C., Wang, H., 2005. Characteristics and pozzolanic reactivity of glass powders 35, 987–993. https://doi.org/10.1016/j.cemconres.2004.05.015

Sing KS., 1985. Reporting Physisorption data for gas/solid systems Pure and Applied Chemistry. Fundam. Adsorpt. Proc. Eng. Found. Conf. Bavaria, West Ger, Eng. Found. 16, 72. 57, 603–619.

Taha, B., Nounu, G., 2009. Utilizing Waste Recycled Glass as Sand/Cement Replacement in Concrete. J. Mater. Civ. Eng. 21, 709–721. https://doi.org/10.1061/(ASCE)0899-1561(2009)21:12(709)

Taha, B., Nounu, G., 2008. Properties of concrete contains mixed colour waste recycled glass as sand and cement replacement. Constr. Build. Mater. 22, 713–720. https://doi.org/10.1016/j.conbuildmat.2007.01.019

Tan, K.H., Du, H., 2013. Use of waste glass as sand in mortar: Part i - Fresh, mechanical and durability properties. Cem. Concr. Compos. 35, 118–126. https://doi.org/10.1016/j.cemconcomp.2012.08.028

Urhan, S., 1987a. Alkali silica and pozzolanic reactions in concrete. Part 1: Interpretation of published results and an hypothesis concerning the mechanism. Cem. Concr. Res. 17, 141–152. https://doi.org/10.1016/0008-8846(87)90068-8

787 Urhan, S., 1987b. Alkali silica and pozzolanic reactions in concrete. Part 2: Observations on expanded
788 perlite aggregate concretes. Cem. Concr. Res. 17, 465–477. https://doi.org/10.1016/0008-
789 8846(87)90010-X

790 Vaitkevičius, V., Šerelis, E., Hilbig, H., 2014. The effect of glass powder on the microstructure of
791 ultra high performance concrete. Constr. Build. Mater. 68, 102–109.
792 https://doi.org/10.1016/j.conbuildmat.2014.05.101

793 World Business Council for Sustainable Development and International Energy Agency, 2009.
794 WBCSD (World Business Council for Sustainable Development), IEA (International Energy
795 Agency), Cement Technology Roadmap 2009: Carbon Emissions Reductions up to 2050.

796 Xiao, R., Zhang, Y., Jiang, X., Polaczyk, P., Ma, Y., Huang, B., 2021. Alkali-activated slag
797 supplemented with waste glass powder: Laboratory characterization, thermodynamic modelling
798 and sustainability analysis. J. Clean. Prod. 286, 125554.
799 https://doi.org/10.1016/j.jclepro.2020.125554

800 Xu, Y., Chung, D.D.L., 2000. Cement of high specific heat and high thermal conductivity, obtained by
801 using silane and silica fume as admixtures. Cem. Concr. Res. 30, 1175–1178.
802 https://doi.org/10.1016/S0008-8846(00)00296-9

803 Yang, S., Ling, T.-C., Cui, H., Poon, C.S., 2019. Influence of particle size of glass aggregates on the
804 high temperature properties of dry-mix concrete blocks. Constr. Build. Mater. 209, 522–531.
805 https://doi.org/10.1016/j.conbuildmat.2019.03.131

806 Younsi, A., Turcry, P., Rozière, E., Aït-Mokhtar, A., Loukili, A., 2011. Performance-based design and
807 carbonation of concrete with high fly ash content. Cem. Concr. Compos. 33, 993–1000.
808 https://doi.org/10.1016/j.cemconcomp.2011.07.005

809 Zemri, C., Bachir Bouiadjra, M., 2020. Comparison between physical–mechanical properties of mortar
810 made with Portland cement (CEMI) and slag cement (CEMIII) subjected to elevated
811 temperature. Case Stud. Constr. Mater. 12, e00339. https://doi.org/10.1016/j.cscm.2020.e00339

812 Zidol, A., Pavoine, A. and Tagnit-Hamou, A., 2012. Effect of Glass Powder on Concrete Permeability.
813 Int. Congr. Concr. Durability, Trondheim, Norw. 15.

814 Zidol, A., 2009. Optimisation de la finesse de la poudre de verre dans les systèmes cimentaires
815 binaires. Master's Thesis. University of Sherbrooke, Canada.

816 Zidol, A., Tognonvi, M.T., Tagnit-Hamou, A., 2017. Effect of Glass Powder on Concrete
817 Sustainability. New J. Glas. Ceram. 07, 34–47. https://doi.org/10.4236/njgc.2017.72004

818